the plant journal

SEB SOCIETY FOR EXPERIMENTAL BIOLOGY

The Plant Journal (2022) **109,** 295–313 doi: 10.1111/tpj.15551

TECHNICAL ADVANCE

A hybrid kinetic and constraint-based model of leaf metabolism allows predictions of metabolic fluxes in different environments

Sanu Shameer[1,†], Yu Wang[2,†], Pedro Bota[1], R. George Ratcliffe[1], Stephen P. Long[2,3] and Lee J. Sweetlove[1,*]

[1]*Department of Plant Sciences, University of Oxford, South Parks Road, Oxford OX1 3RB, UK,*

[2]*Carl R Woese Institute for Genomic Biology, University of Illinois at Urbana-Champaign, Urbana, IL 61801, USA, and*

[3]*Lancaster Environment Centre, Lancaster University, Lancaster LA1 4YQ, UK*

Received 12 March 2021; revised 8 October 2021; accepted 20 October 2021; published online 26 October 2021.

*For correspondence (e-mail lee.sweetlove@plants.ox.ac.uk).

†These authors contributed equally to this work.

SUMMARY

While flux balance analysis (FBA) provides a framework for predicting steady-state leaf metabolic network fluxes, it does not readily capture the response to environmental variables without being coupled to other modelling formulations. To address this, we coupled an FBA model of 903 reactions of soybean (*Glycine max*) leaf metabolism with e-photosynthesis, a dynamic model that captures the kinetics of 126 reactions of photosynthesis and associated chloroplast carbon metabolism. Successful coupling was achieved in an iterative formulation in which fluxes from e-photosynthesis were used to constrain the FBA model and then, in turn, fluxes computed from the FBA model used to update parameters in e-photosynthesis. This process was repeated until common fluxes in the two models converged. Coupling did not hamper the ability of the kinetic module to accurately predict the carbon assimilation rate, photosystem II electron flux, and starch accumulation of field-grown soybean at two CO_2 concentrations. The coupled model also allowed accurate predictions of additional parameters such as nocturnal respiration, as well as analysis of the effect of light intensity and elevated CO_2 on leaf metabolism. Predictions included an unexpected decrease in the rate of export of sucrose from the leaf at high light, due to altered starch–sucrose partitioning, and altered daytime flux modes in the tricarboxylic acid cycle at elevated CO_2. Mitochondrial fluxes were notably different between growing and mature leaves, with greater anaplerotic, tricarboxylic acid cycle and mitochondrial ATP synthase fluxes predicted in the former, primarily to provide carbon skeletons and energy for protein synthesis.

Keywords: technical advance, metabolic modelling, flux balance analysis, kinetic modelling, *Glycine max*, central carbon metabolism.

INTRODUCTION

Improving the efficiency of photosynthesis has been proposed as a feasible, and underexploited, means to increase crop yield (Long et al., 2019; Zhu et al., 2010). Recent attempts to engineer increased photosynthetic rates have resulted in improved crop productivity in field trials, providing successful test-of-concept (Kromdijk et al., 2016; López-Calcagno et al., 2020; South et al., 2019; Yoon et al., 2020). Despite these successes, the photosynthetic energy conversion efficiency (ε_c; the fraction of intercepted radiation converted into plant mass) of current improvements is still far from the theoretical maximum (Long et al., 2019; Zhu et al., 2008, 2010). Successful intervention to increase ε_c depends on our understanding of the biochemical limitations of photosynthetic energy conversion. This is challenging because photosynthesis is directly or indirectly affected by other metabolic pathways (Paul and Foyer, 2001; Paul and Pellny, 2003).

Mathematical modelling is a powerful approach for understanding the photosynthetic process. Farquhar et al. (1980) developed a steady-state model of C_3 photosynthesis, which assumes photosynthesis cannot proceed faster than the limit set by the carboxylase activity or the electron transport rate. This model has been used to predict steady-

state CO_2 assimilation rates and has proved robust under various environmental conditions, including light intensity, $[CO_2]$ and $[O_2]$. The Farquhar model and its later versions have been extensively used in other models of leaf metabolism (Caemmerer, 2000; Heckmann et al., 2013; Yin and Struik, 2009). It is also commonly implemented as a submodule in multi-scale models such as crop growth models and land surface exchange models (Cox et al., 1999; Miguez et al., 2009; Sellers et al., 1996; Vos et al., 2010). However, the Farquhar model does not describe the individual metabolic reactions of photosynthesis, and so it cannot be used directly to study the fluxes through the leaf metabolic network or the impact of manipulating individual photosynthetic enzymes on the efficiency of the whole metabolic system. For insights into these processes, it is necessary to turn to other metabolic modelling approaches, such as constraint-based modelling and kinetic modelling.

Constraint-based modelling is a metabolic modelling approach that uses a set of physical, biochemical, and thermodynamic constraints to define a solution space that describes all feasible flux distributions supported by a system of metabolic reactions of defined stoichiometry. This modelling approach does not require enzyme/metabolite concentrations or kinetic parameters (Beard and Qian, 2005). The most commonly implemented formulation, flux balance analysis (FBA), has been extensively used to study leaf metabolism in C_3 plants (Arnold and Nikoloski, 2014; Chatterjee et al., 2017; Cheung et al., 2014, 2015; de Oliveira Dal'Molin et al., 2010; Herrmann et al., 2019; Lakshmanan et al., 2015; Mintz-Oron et al., 2012; Poolman et al., 2013; Shameer et al., 2019; Yuan et al., 2016). FBA is capable of modelling steady-state metabolic fluxes in stoichiometric models (Orth et al., 2010), and current FBA leaf models are capable of modelling photosynthesis in growing and fully expanded leaves. It is possible to include both day- and night-time metabolism in the model, providing a more accurate description of leaf metabolism over the diel cycle (Cheung et al., 2014; Töpfer et al., 2020).

FBA models are based on reaction stoichiometries and require only a few biochemical and thermodynamic constraints. As a result, these models can be used to simulate flux distributions through extremely large metabolic networks, even genome-scale metabolic networks composed of more than 8000 reactions and metabolites, in a computationally efficient manner (Simons et al., 2014). FBA models are composed of linear equations and while this makes them computationally efficient, most biological processes are non-linear and FBA models are unable to represent these non-linear processes directly. This makes it difficult to directly account for the complex relationship between kinetic parameters such as K_M, metabolite concentrations, and flux within the FBA framework.

As a result, FBA models need additional components to capture the non-linear responses to changes in light and other environmental variables. For example, environment-specific biomass compositions (Arnold and Nikoloski, 2014; Poolman et al., 2013), maximum enzymatic activity (Recht et al., 2014), transcriptomics data (Imam et al., 2015; Kamsen et al., 2021; Mintz-Oron et al., 2012; Scheunmann et al., 2018; Siriwach et al., 2020), and metabolomics data (Kleessen et al., 2015; Pries et al., 2021; Sajitz-Hermstein et al., 2016) have all been used to constrain FBA models in response to changes in light, atmospheric CO_2 concentration, nutrient availability, and other environmental variables. While these approaches have been shown to improve the predictive power of constraint-based models, they rely heavily on the availability of context-specific data to model the non-linear metabolic responses.

Dynamic FBA (dFBA) is another approach that can account for the non-linear nature of metabolism. The simplest formalism of dFBA, the static optimization algorithm, involves monitoring concentrations of specific metabolites during an FBA run, and then using ordinary differential equations (ODEs) to introduce constraints on appropriate reaction fluxes for the subsequent FBA run (Grafahrend-Belau et al., 2013; Schroeder and Saha, 2020; Shaw and Cheung, 2018). More complicated formalisms of dFBA, dynamic optimization algorithms, trade off the steady-state assumption responsible for maintaining the linear nature of these models for improved representation of the dynamics of metabolic systems. A comprehensive review of dynamic optimization algorithms has been presented in Kleessen and Nikoloski (2012).

Non-linear processes can be captured explicitly in kinetic modelling, which uses a mathematical representation of reactions in a metabolic network based on rate equations that account for enzyme kinetics and metabolite concentrations. Kinetic models, such as those composed of ODEs, are capable of simulating not only the steady-state fluxes of the system, but also the dynamic response of reactions to environmental changes. Many kinetic models of leaf metabolism focus on photosynthesis and pathways of related carbon metabolism (Cox et al., 1999; Fridlyand and Scheibe, 1999; Gombert and Nielsen, 2000; Laisk and Walker, 1986; Laisk et al., 1989; McGrath and Long, 2014; Miguez et al., 2009; Morales et al., 2018; Pearcy et al., 1997; Poolman et al., 2000; Sellers et al., 1996; Vos et al., 2010; Wang et al., 2014; Woodrow and Mott, 1993; Zaks et al., 2012; Zhu et al., 2007, 2013). These range from models describing photosynthesis by two processes (Farquhar et al., 1980) to models representing all discrete steps in the process, combined with light activation/deactivation of enzymes (Zhu et al., 2013). The ambition is to extend the metabolic reach of these models, and most recently a model has been assembled that includes glycolysis, gluconeogenesis, the tricarboxylic acid (TCA) cycle, and chloroplastic nitrogen assimilation, as well as the Calvin cycle, the photorespiration pathway, and starch

synthesis (Zhao et al., 2021), Kinetic models have been used to analyse the control of both steady-state and transient properties of photosynthesis, and to identify potential targets for photosynthesis and yield improvement. However, it can be difficult to obtain accurate measurements of all the kinetic parameters required for large-scale ODE models; and numerical integration of ODE systems can be challenging due to the different time scales of processes within the model.

Hybrid models composed of ODE and FBA models have been proposed as a way of addressing the limitations of both types of modelling, leading to a more accurate modelling framework that remains computationally tractable. Inclusion of kinetic equations based on a power-law formalism for key branch points of the metabolic network was shown to improve the predictive power of an FBA model of microbial glycolysis (Pozo et al., 2015). The first steps in this direction have also been taken for leaf metabolic models. For example, in a constraint-based model of metabolism across the C_3–C_4 gradient of the maize leaf, sub-models of gas-diffusion and RuBisCo kinetics were used to compute and constrain ribulose-1,5-bisphosphate (RuBP) carboxylation to oxygenation ratio in the FBA model (Bogart and Myers, 2016). Similarly, Heckmann et al. (2013) used non-linear sub-models to constrain net CO_2 uptake, RuBisCo activity, bundle-sheath CO_2 leakage, mesophyll phospho*enol*pyruvate carboxylase (PEPC), bundle-sheath C_4 acid decarboxylation, glycine decarboxylase, and the exchange of glycine and serine between bundle sheath and mesophyll to constrain fluxes in the C4GEM constraint-based model (Oliveira Dal'Molin et al., 2010).

Here, we describe a hybrid leaf model of unprecedented scale, constructed by combining a previously established ODE model of all discrete steps of photosynthetic metabolism, the e-photosynthesis ODE model (Zhu et al., 2013), with an FBA model of diel leaf metabolism (Shameer et al., 2019). We explore two ways of integrating the two models: a general loosely coupled approach (LC-ODE-FBA) and a tailored tightly coupled approach (TC-ODE-FBA). We show how the latter approach, while more time-consuming to develop and execute, is capable of capitalizing on the strengths of the individual models while minimizing their weaknesses. Accurate flux predictions of key photosynthetic parameters such as CO_2 assimilation rate, photosystem II (PSII) flux and starch accumulation are retained by the coupled model, which can make predictions such as the effect of elevated CO_2 on nocturnal respiration rate, and are consistent with the measurements of field-grown soybean plants. The broader behaviour of soybean leaf metabolism under three different light intensities, at elevated atmospheric [CO_2], and in growing versus mature source leaves was explored using the TC-ODE-FBA model.

RESULTS

LC-ODE-FBA model design

The simplest approach to integrating the e-photosynthesis model (the ODE model) and a diel leaf FBA model is to use the fluxes predicted by the more mechanistic ODE model to constrain the solution space of the FBA model. This was implemented in the LC-ODE-FBA model consisting of two modules, the ODE module (e-photosynthesis model) and an FBA module. The ODE module was run first and the predicted values for the PSII electron flux (J_{PSII}) and the ribulose-1,5-bisphosphate carboxylation–oxygenation flux ratio (V_c/V_o) were extracted for a given light intensity and atmospheric [CO_2]. These values were then used to constrain the flux of the corresponding reactions in the diel FBA model (Figure 1). The ODE and FBA modules were formulated as described in the model execution section and values were passed between them using yggdrasil, a Python package for integrating models across languages and scales, while coordinating their parallel execution (Lang, 2019).

TC-ODE-FBA model design

The LC-ODE-FBA model transfers only two of the ODE-predicted fluxes to the FBA module. An alternative approach is to allow the ODE module to predict fluxes through all the chloroplast metabolic reactions, and then to use the FBA model to predict flux through the chloroplast reactions that were unaccounted for in the ODE model, such as amino acid and lipid synthesis, as well as the reactions in the other subcellular compartments. In this TC-ODE-FBA model, the additional chloroplast ATP and reducing power costs from the FBA model need to be accounted within the ODE model (Figure 2).

The ODE module consisted of the soybean e-photosynthesis model, which was modified to account for any additional daytime chloroplast ATP and NADPH costs observed in the FBA module. This was achieved by introducing an additional ATP sink term (v_{ATP_ODE}) to the equation representing the rate of change of chloroplast ATP concentration in the ODE model:

$$d[ATP]'_{Chl}/dt = d[ATP]_{Chl}/dt - v_{ATP\_ODE} \quad (1)$$

Similarly, an NADPH sink term (v_{NADPH_ODE}) was added to the equation representing the rate of change of NADPH in the chloroplast to account for the extra NADPH costs:

$$d[NADPH]'_{Chl}/dt = d[NADPH]_{Chl}/dt - v_{NADP\_ODE} \quad (2)$$

To represent the flow of metabolites between the ODE model and the FBA model, exchange reactions (reactions that represent the import or export of metabolites into or out of the model) were added for cytosolic triose-phosphate (TP), cytosolic 3-phosphoglycerate (PGA), cytosolic inorganic phosphate, cytosolic glycolate, and

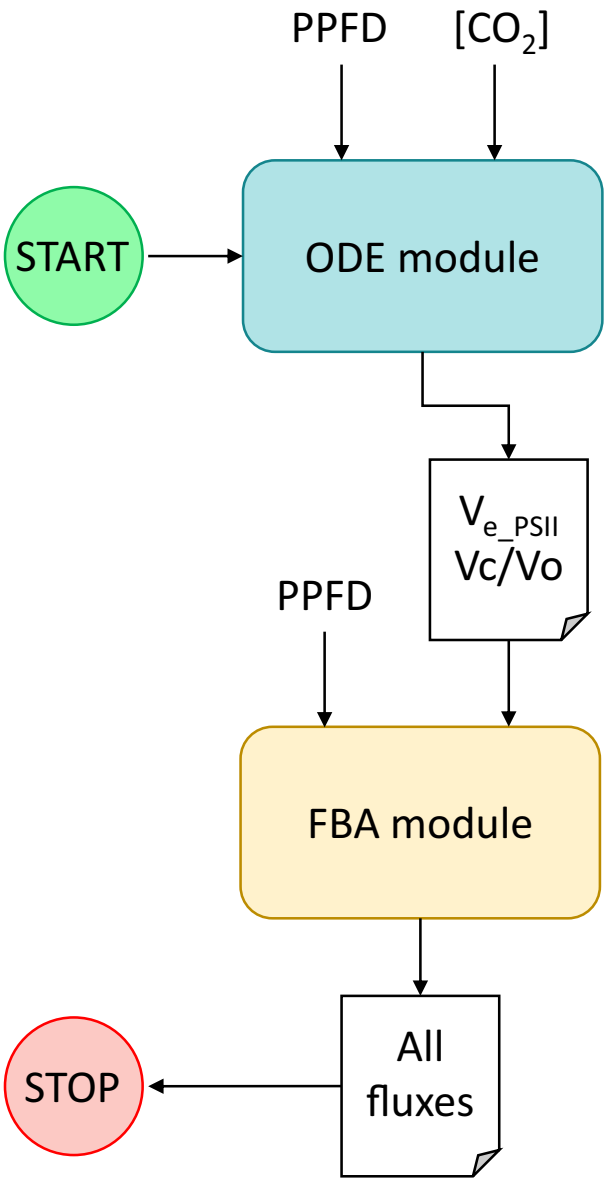

Figure 1. The loosely coupled ordinary differential equation (ODE)–flux balance analysis (FBA) model.
The e-photosynthesis ODE model and diel leaf FBA models can be combined in a loosely coupled configuration model of leaf metabolism. The ODE module is used to predict photosystem II electron flux (V_{e_PSII}) and the RuBisCo-catalysed ribulose-1,5-bisphosphate carboxylation-oxygenation ratio (V_c/V_o) for a given photon influx rate [photosynthetic photon flux density (PPFD)] and atmospheric [CO_2]. The diel leaf FBA module, constrained by the values of V_{e_PSII} and V_c/V_o, is used to predict the leaf metabolic network fluxes under the same conditions.

cytosolic glycerate. Exchange reactions for vacuolar malate and vacuolar citrate were also added to the FBA model to enable it to represent organic acid accumulation and remobilization fluxes. To allow the ODE model to supply ATP and NADPH to the FBA chloroplast, reactions for chloroplast ATP and NADPH generation from ADP and NADP+ respectively, were added to the FBA model. To ensure that there was no duplication of fluxes between the ODE and FBA models, metabolic pathways already accounted for by the ODE model were constrained to zero flux in the FBA model. Hence, the FBA chloroplast does not have active reactions for the photosynthetic light reactions, CO_2 fixation by RuBisCo, photorespiration, or starch biosynthesis. However, all other chloroplast reactions in the FBA model, principally those involved in amino acid biosynthesis, were free to carry fluxes.

The TC-ODE-FBA formulation does not use a diel FBA model, because the ODE model only accounts for chloroplast metabolism in the light, i.e., when photosynthesis is occurring. This means that the FBA model needed to be constrained to force it to accumulate malate and remobilize citrate during the day. From separate diel FBA leaf model predictions, the following relationships between starch accumulation and organic acid accumulation/remobilization were noted (Table S1):

$$V_{MAL\_acc} = 0.71 \times V_{STARCH\_acc} \quad (3)$$

$$V_{CIT\_acc} = -0.56 \times V_{STARCH\_acc} \quad (4)$$

where V_{MAL_acc}, V_{CIT_acc}, and V_{STARCH_acc} are malate, citrate, and starch accumulation fluxes for which positive values suggest accumulation and negative values suggest remobilization of accumulated metabolites. These equations were used to constrain the respective fluxes in the FBA model. A complete list of all constraints used to set-up the daytime leaf FBA model for TC-ODE-FBA is presented in Table S2.

To run the TC-ODE-FBA model, the initial values for v_{ATP_ODE} and v_{NADPH_ODE} were set to 0, and the steady-state values predicted by the ODE module for chloroplast TP and PGA export and starch accumulation rate were recorded. In the FBA module, the exchange reactions for TP and PGA were constrained to the values recorded in the ODE module. Likewise, the values for the chloroplast glycolate efflux and glycerate influx predicted by the ODE module were used to constrain the equivalent exchange fluxes in the FBA model. These constraints ensured that while the ODE module of TC-ODE-FBA was responsible for the chloroplastic parts of the photorespiratory flux, the remainder of the pathway (glycerate generation from glycolate) was left to the FBA component. The rate of starch accumulation in the ODE model was also used to constrain malate accumulation and citrate remobilization rates in the vacuole of the FBA model based on equations (3) and (4), respectively. Fluxes through reactions generating ATP and NADPH in the FBA model were constrained based on v_{ATP_ODE} and v_{NADPH_ODE} fluxes from the ODE module. Parsimonious FBA (pFBA) was then used to predict a flux distribution in the FBA model that maximized the export of sucrose and amino acids from the leaf to the phloem. A feasible solution was guaranteed because there were no

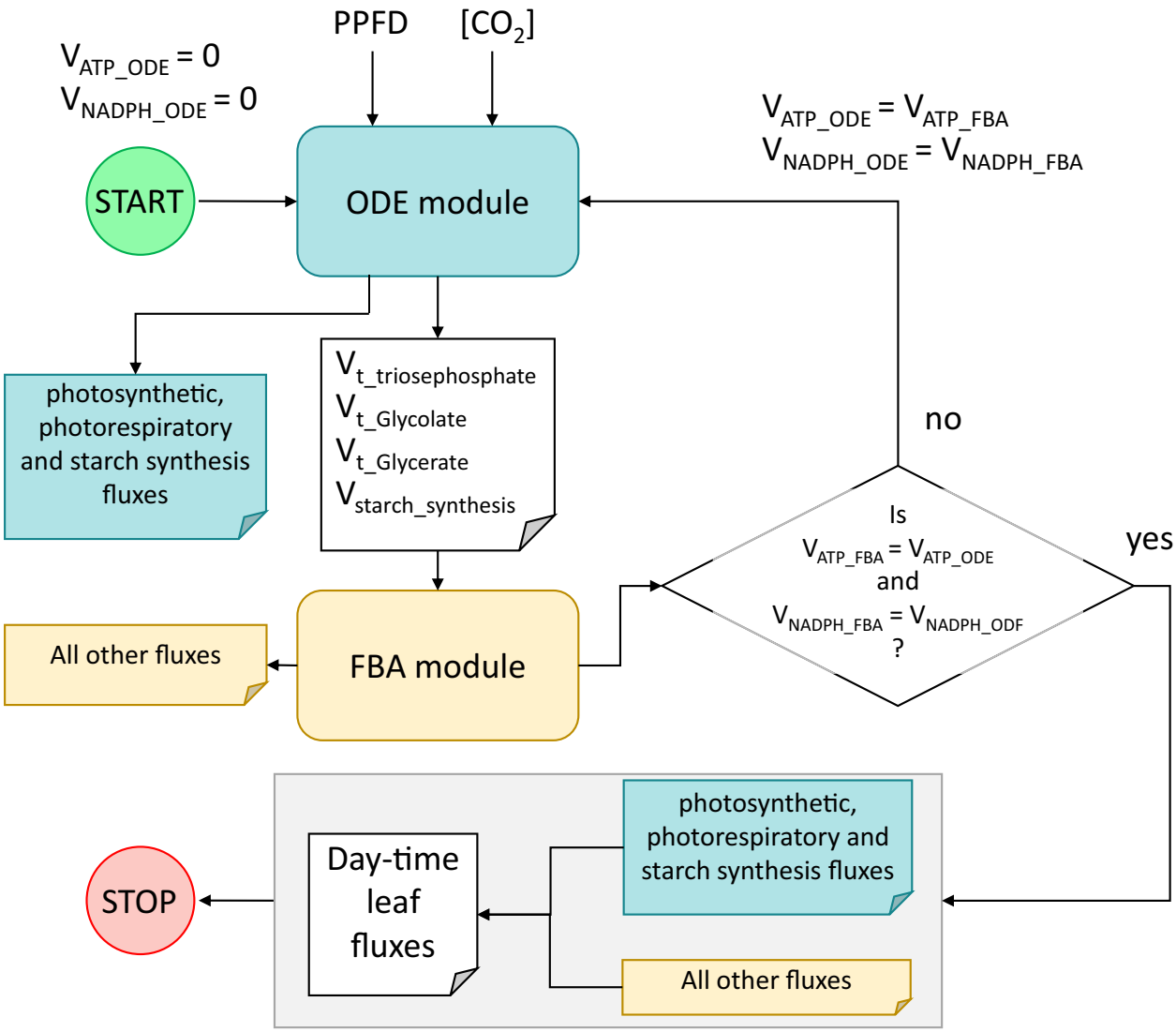

Figure 2. The tightly coupled ordinary differential equation (ODE)–flux balance analysis (FBA) model.
In the tightly coupled configuration, the ODE module is used to model photosynthetic, photorespiratory, and starch synthesis fluxes for a given light intensity [photosynthetic photon flux density (PPFD)] and atmospheric [CO_2]. The chloroplast triose-phosphate efflux ($V_{t\_triosephosphate}$), glycolate efflux ($V_{t\_glycolate}$), glycerate influx ($V_{t\_glycerate}$), and starch accumulation rate ($V_{starch\_synthesis}$) predicted from the ODE module were used as inputs and constraints on the FBA module. V_{ATP_ODE} and V_{NADPH_ODE} represent energy sink fluxes accounting for the additional ATP and NADPH costs arising from plastid metabolism beyond the ODE module. V_{ATP_FBA} and V_{NADPH_FBA} represents the net ATP and NADPH demand of the plastid in the FBA module. ODE and FBA models were run in a loop until all plastidic ATP and NAD(P)H demands in the FBA model were met by the ODE model.

obligatory demands on the FBA model other than the non-growth associated maintenance (NGAM), which was constrained as a function of light intensity (Töpfer et al., 2020), and hence the ODE steady-state solution for the same light intensity should fall within FBA solution space.

The fluxes through the ATP and NAD(P)H shuttles [plastid nucleotide transporter (NTT) and malate dehydrogenase (MDH) activity respectively] to the chloroplast in the FBA module were observed to check whether the chloroplast ATP and NADPH demands in the FBA model were met by the ODE model. As flux variability analysis revealed that ATP shuttling via NTT and PEP-pyruvate shuttle contributed equally to the optimization problem, the flux weighting on the NTT reaction was changed from 1 to 0.5 during the minimization of sum of fluxes stage of pFBA to ensure that all the ATP was shuttled via the NTT reaction during pFBA. From the pFBA run, the net ATP demand of the chloroplast, v_{ATP_FBA} (equivalent to ATP available from v_{ATP_ODE} and NTT) and the net NADPH demand of the chloroplast, v_{NADPH_FBA} (equivalent to NADPH available from v_{NADPH_ODE} and MDH) were recorded. If the shuttles were found to be actively importing ATP or NAD(P)H into the FBA chloroplasts, then the values of v_{ATP_ODE} and v_{NADPH_ODE} were updated to v_{ATP_FBA} and v_{NADPH_FBA},

respectively, to account for the ATP and NADPH shuttled; and the ODE and FBA modules were run again. Only when the net ATP and NADPH demand in the FBA chloroplast were found to be met by the ODE model (i.e. v_{ATP_FBA} ~= v_{ATP_ODE} and v_{NADPH_FBA} ~= v_{NADPH_ODE}, a difference <0.005 was considered negligible), were the ODE and FBA (representing daytime metabolism) models deemed to have reached a consensus. The loop was then broken and fluxes for daytime metabolism from both modules were recorded.

Night-time leaf metabolism in the TC-ODE-FBA set-up was modelled using another copy of the soy-specific PLANTCOREMETABOLISM FBA model. This model was set up by setting photon uptake to zero and constraining starch degradation, malate remobilization, and citrate accumulation rates based on total starch accumulated during the photoperiod, such that at dawn all the accumulated starch was depleted. A complete list of all constraints used to set-up the night-time leaf FBA model for TC-ODE-FBA is presented in Table S3. Again, pFBA was used to model fluxes maximizing the night-time export of sucrose and amino acids from the leaf to the phloem. As with the LC-ODE-FBA model, ODE and FBA modules were formulated as described in the model execution section and integrated for the TC model using the yggdrasil framework (Lang, 2019).

Coupled-ODE-FBA models make accurate predictions of the effect of light intensity and atmospheric [CO_2] on photosynthetic assimilation rate

The e-photosynthesis ODE model accurately accounts for the effect of atmospheric [CO_2] and light intensity, with the model-predicted rate of photosynthetic carbon assimilation closely matching experimentally measured values (Figure 3a,b). In contrast, the FBA model fails to reflect changes in atmospheric [CO_2] and light intensity: the predicted photosynthetic assimilation rate is insensitive to [CO_2] (Figure 3a) and the model predicts a linear response to light intensity (Figure 3b). Figure 3 also shows that the ODE, LC-ODE-FBA, and TC-ODE-FBA models predicted very similar *A* values to each other across a range of light intensities and atmospheric [CO_2] with the coupled models predicting *A* values slightly lower than the ODE model, although still close to experimental values. Because the PSII electron flux is constrained to the corresponding flux in the ODE model, both ODE and LC-ODE-FBA models carry the same flux through their respective photosynthetic linear electron flow (LEF) pathways, generating the same amount of reducing power for a given light intensity. The LC-ODE-FBA model, however, has additional reducing power demands when compared with the ODE model (maintenance and photorespiratory N-refixation), so it predicts lower *A* values. The TC-ODE-FBA model also predicts slightly lower *A* values compared with the ODE model because of the higher ATP and reducing power demand due to accounting for maintenance, photorespiratory N-refixation, and sucrose biosynthesis (see Data S1, S2). Maintenance costs (defined in the FBA component) were observed to decrease TC-ODE-FBA assimilation rate by 11% in saturating light (HL) conditions. Predicted *A* values from both coupled models fell within the range of *A* values reported in previously published experiments (Figure 3a,b).

While both coupled models predicted very similar *A* values, there is a major difference in the energetic flexibility of the two models. In the LC-ODE-FBA model, LEF (handled by the FBA module) is limited by the PSII electron flux predicted by the ODE module, but the model is free to run unconstrained cyclic electron flow (CEF) to generate additional ATP to meet its energy demands (as is evident from

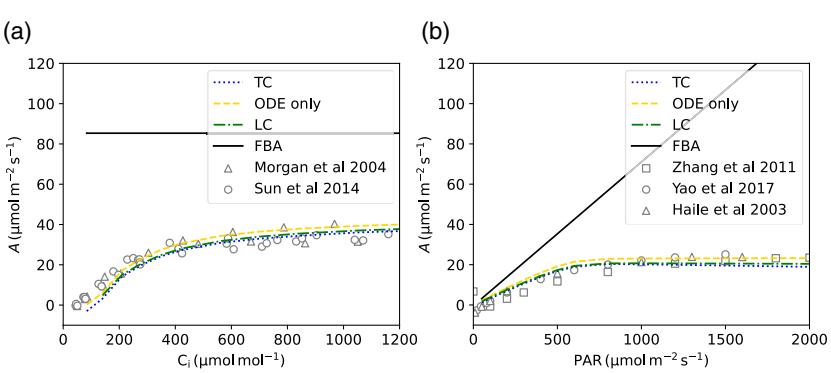

Figure 3. Predicted and experimental dependence of gross leaf CO_2 assimilation on intercellular CO_2 [C_i] and incident light flux [photosynthetic photon flux density (PPFD)].
(a) Predicted and experimental *A*-Ci curves from the flux balance analysis (FBA) and ordinary differential equation (ODE) models alone and the loosely (LC) and tightly coupled (TC) ODE-FBA models. Light intensity was 1200 μmol m^{-2} sec^{-1}. Triangle and circle symbols show *A*-*Ci* field data measured at saturated light intensity from Morgan et al. (2004) and Sun et al. (2014), respectively.
(b) Predicted *A*-PPFD curves from the FBA, ODE, LC, and TC ODE-FBA models. Atmospheric [CO_2] was 400 ppm. Circle, triangle and square symbols represent measurements at ambient CO_2 from Haile and Higley (2003), Yao et al. (2017), and Zhang et al. (2011), respectively.

the 'Ferredoxin_Plastoquinone_Reductase_p1' flux in Data S3). In contrast, in the TC-ODE-FBA model the relative rates of LEF and CEF are dictated by the kinetic parameters of the relevant photosynthetic electron transport chain complexes and this results in a more limited ATP supply from photons. Hence, the TC-ODE-FBA model predicted utilization of the TCA cycle and mitochondrial ATP synthesis to meet the remainder of its ATP demand. For example, when modelling metabolism in leaves grown in a 1000 μmol m^{-2} sec^{-1} light intensity and 400 ppm [CO_2], the LC-ODE-FBA model gave a CEF/LEF ratio of 0.45 compared with a value of 0.33 in the TC-ODE-FBA model. On the other hand, the LC-ODE-FBA model did not predict any mitochondrial ATP synthesis compared with a value of 7.24 μmol ATP m^{-2} sec^{-1} in the TC-ODE-FBA model. The LC-ODE-FBA and TC-ODE-FBA models also showed a significant difference regarding run-times. While the LC-ODE-FBA model only needed to run its ODE and FBA components once, the TC-ODE-FBA model needs to run until both its ODE and FBA components achieved convergence, which was noted to happen within four to 10 cycles, resulting in the TC-ODE-FBA model taking four to 10 times longer to run than the LC-ODE-FBA model (Figure S1). A summary of the different capabilities of the ODE, FBA, LC-ODE-FBA, and TC-ODE-FBA models is presented in Table S4.

Comparing predicted rates of photosynthesis and starch synthesis with measured data

The predictive accuracy of the coupled ODE-FBA models was assessed by comparing the predicted rates of CO_2 assimilation, PSII electron transport flux, and starch accumulation in the FBA, ODE, LC-ODE-FBA, and TC-ODE-FBA models with experimental data from soybean grown in free air CO_2 enrichment (FACE) experiments (Rogers et al., 2004). The predicted fluxes from each model are listed in Data S1–S4. The FBA model substantially overestimated *A*, while the ODE model, LC-ODE-FBA, and TC-ODE-FBA models predicted accurate values for *A* at two different atmospheric CO_2 concentrations (no statistically significant difference from the experimentally measured data) (Figure 4a). Similarly, all the models except the FBA model, accurately predicted J_{PSII} in both ambient and elevated [CO_2] (Figure 4b). Elevated [CO_2] resulted in a higher J_{PSII} than ambient [CO_2], but the proportional increase was much less than for *A* (Figure 4b). Turning to daytime starch accumulation, both the FBA and LC-ODE-FBA models predict lower leaf starch levels at noon compared with the ODE and TC-ODE-FBA models (Figure 4c). However, all predictions were not significantly different from the estimates based on experimental data.

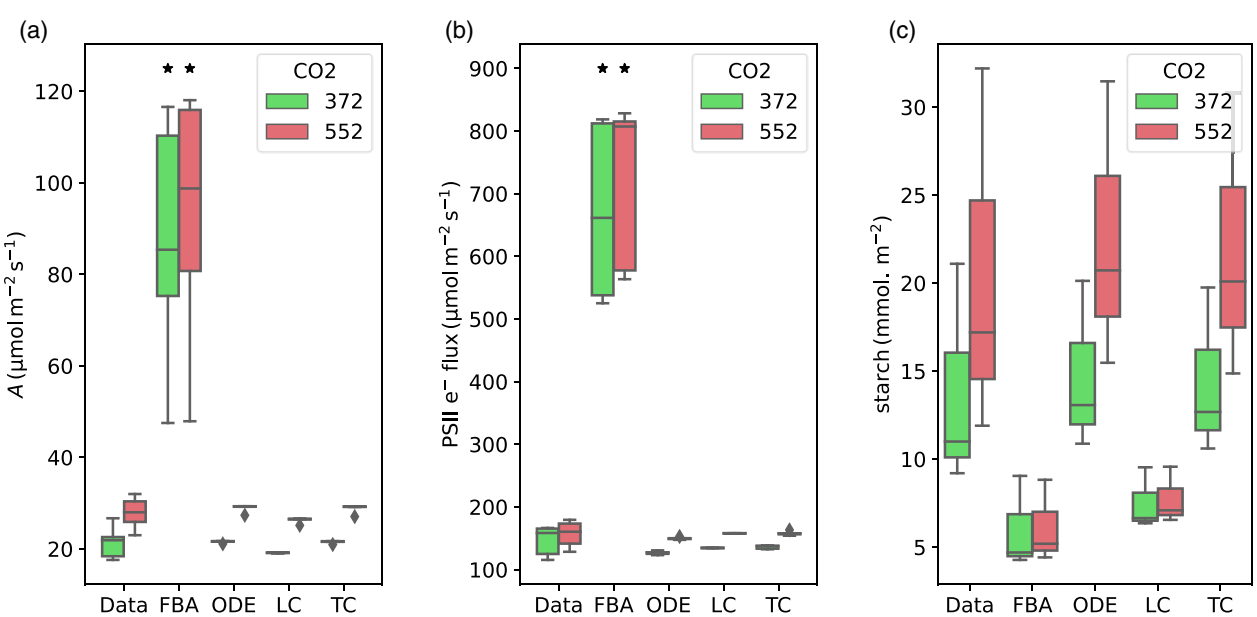

Figure 4. Statistical comparison of model-predicted fluxes with experimentally determined values.
(a) Net CO_2 assimilation flux and (b) the rates of photosystem II (PSII) electron transport (J_{PSII}) predicted by the flux balance analysis (FBA), ordinary differential equation (ODE), tightly coupled (TC)-ODE-FBA and loosely coupled (LC)-ODE-FBA models at noon (6th hour of the photoperiod) on days 164, 176, 191, 205, and 215 of the free air CO_2 enrichment experiment were compared with experimentally measured values reported in Rogers et al. (2004). Measured J_{PSII} from Rogers et al. (2004) was divided by 2 to correct the PSII electron transport rate.
(c) Leaf starch levels at noon on days 191, 205, and 215 were estimated from hourly starch accumulation rates predicted by the models and was compared with experimentally determined values from Rogers et al. (2004). For each simulation, only [CO_2] and light intensity were changed according to the measured values. Box plot whiskers represent the extremes in the data. Paired Student's *t*-tests were performed to determine if the means of each model simulation set and the measured values were significantly different from each other. $*P < 0.001$.

The improved prediction accuracy for starch accumulation by the TC-ODE-FBA model can be attributed to the fact that it utilizes the ODE module to predict starch accumulation rates by accounting for the kinetics of photoassimilate partitioning. The LC-ODE-FBA model, on the other hand, relies on the FBA component to predict the starch accumulation rate, which is significantly influenced by model parameters such as maintenance costs and the day/night phloem export rate ratio. However, these parameters were not based on soy data and so the predicted starch accumulation rate is less likely to be accurate.

A parameter sensitivity analysis was undertaken to test the robustness of the predictive accuracy of the TC-ODE-FBA model to the various parameter choices and assumptions contained within the model (Information S1, Table S5). Key assumptions and parameters in the FBA module, such as the maintenance cost, the constraint on the ratio of starch to carboxylic acid accumulation, and the constraint on phloem metabolite composition, had negligible effects on the accuracy with which the TC-ODE-FBA model predicted *A* and starch accumulation at both ambient and elevated [CO_2]. In contrast, varying 14 of the 309 kinetic parameters by $\pm$50% was noted to impact the TC-ODE-FBA model CO_2 assimilation rate predictions (and hence the ability of the model to predict leaf starch content as well). An additional two kinetic parameters were observed to influence starch accumulation rate predictions significantly (Table S5). While overall, this demonstrates that the model is robust to small variations in the parameters used, it also highlights, sensitivity to a small number of the kinetic parameters. Future work could look to determining more accurate values for these specific parameters and checking that they do not change in soybean plants grown under different environments.

TC-ODE-FBA model predicts a higher night-time respiration rate in soybean grown under elevated [CO_2]

The TC-ODE-FBA model can be used to model night-time leaf metabolism using the outputs from the daytime model and a single-phase nocturnal FBA module. The FBA module predicted that the oxidative pentose phosphate pathway (PPP) and pyruvate dehydrogenase (PDH) were responsible for a significant fraction of night-time CO_2 evolution, with only a small fraction of total CO_2 evolved originating from the TCA cycle. This was found to be a consequence of the organic acid accumulation/remobilization constraints in the model (equations 3 and 4). Malate remobilized from the vacuole was oxidized to oxaloacetate via malate dehydrogenase, contributing to a significant fraction of the TCA flux. A small fraction of this malate was also used to generate pyruvate via malic enzyme. A significant fraction of the citrate generated in the TCA cycle was observed to accumulate in the vacuole to comply with the citrate accumulation constraints. Because of this, a considerably smaller flux was observed in the remainder of the TCA cycle (citrate to malate).

The TC-ODE-FBA model was used to predict the effect of the atmospheric [CO_2] on respiratory CO_2 production in soybean leaves, using parameters from a soybean FACE experiment. The TC-ODE-FBA model predicted a higher respiration rate under elevated CO_2 (Figure 5) consistent with what has been observed experimentally (Rogers et al., 2004). A parameter sensitivity analysis (Information S1, Table S5) showed that in all cases where a model solution was achieved, a higher respiration rate was observed under elevated CO_2 if the same parameter value was used at both CO_2 levels. Table 1 lists fluxes through all the metabolic processes involved in the production and consumption of CO_2 in leaves at night on day 164 of the FACE experiment as modelled by the TC model. Here we see a higher PDH and malic enzyme flux in elevated [CO_2] compared with the ambient conditions. The model proposes this because of the increased availability of vacuolar malate in elevated [CO_2] (a consequence of equation 3 and increased daytime starch accumulation rate predicted by the ODE module; Figure 4c). With increased reducing power being generated by PDH and malic enzyme, oxidative PPP flux was observed to drop in elevated [CO_2] conditions. There was also a predicted decrease in the TCA cycle flux from citrate to malate. The latter also reflected the increased citrate accumulation flux (a consequence of

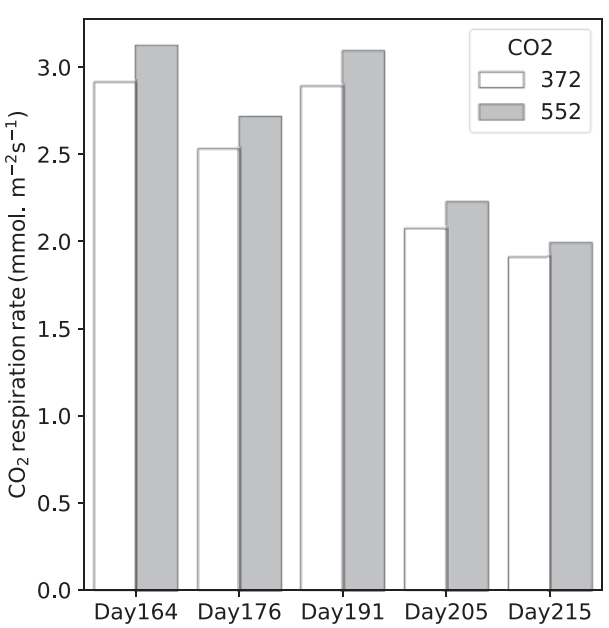

Figure 5. The tightly coupled ordinary differential equation (ODE)–flux balance analysis (FBA) model predicts a higher night-time respiration rate in elevated [CO_2].
The tightly coupled ODE-FBA model was used to model night-time metabolism under ambient and high [CO_2] free air CO_2 enrichment conditions (days 164, 176, 191, 205, and 215) and flux representing net CO_2 expelled from the model (CO2_tx) was extracted from the predicted flux distribution.

Table 1 Night-time CO_2 producing and consuming processes in leaves modelled under day 164 free air CO_2 enrichment conditions

Metabolic process	CO_2 flux (μmol m^{-2} sec^{-1})	
	$[CO_2]$ = 372 ppm	$[CO_2]$ = 552 ppm
Pentose phosphate pathway	1.28	1.10
Pyruvate dehydrogenase	1.09	1.54
TCA cycle	0.27	0.05
Malic enzyme	0.22	0.33
Allantoin degradation	0.03	0.06
Amino acid biosynthesis	0.02	0.04
CO_2 respiration	–2.91	3.12

TCA, tricarboxylic acid.

equation 4 and increased daytime starch accumulation rate predicted by the ODE module; Figure 4c). Overall, a higher respiration rate at elevated CO_2 was observed through increased night-time leaf metabolic activity, which was a consequence of the higher transitory starch store predicted by the ODE component of the hybrid model in elevated CO_2 conditions.

Metabolism under different light intensity and $[CO_2]$ conditions

The TC-ODE-FBA model was used to model the effect of light intensity on daytime metabolism in ambient $[CO_2]$ under low light (LL), medium light (ML), and HL conditions (300, 600, and 1000 μmol photons m^{-2} sec^{-1}, respectively). Major fluxes (those above a threshold of 0.3 μmol m^{-2} sec^{-1}) predicted at LL, ML, and HL are depicted in Figure 6a–c, respectively. Among the many differences, the dissipation of excess light energy, which was primarily via non-photochemical quenching (NPQ), and the fluxes associated with starch accumulation were found to increase with increasing light intensity. The model also predicted sucrose export rates of 0.72, 1.11, and 0.95 μmol m^{-2} sec^{-1} for the LL, ML, and HL conditions, respectively. This pattern was the result of an increased allocation of C towards starch in HL (22% and 39.3% of net assimilated C in ML and HL respectively). The model also predicted a RuBisCo V_c/V_o ratio of 2.96 for all three light conditions, and hence photorespiration and the associated N-refixation fluxes were observed to follow the CO_2 assimilation rate pattern observed in Figure 3b. As NGAM in the model is a function of the incident light intensity, a higher mitochondrial ATP synthase flux (generating ATP to meet NGAM demand) was observed at higher light intensities.

The TC-ODE-FBA model was also used to study the effect of elevated $[CO_2]$ on leaf metabolism by modelling metabolism in 800 ppm $[CO_2]$ and 1000 μmol photon m^{-2}sec^{-1} light intensity (high light, elevated CO_2 [HL-E]; Figure 6d). Compared with HL, HL-E showed decreased photorespiration and an increased Calvin cycle flux resulting in higher chloroplastic ATP and NADPH consumption. As a result, more of the incident light was used for photochemistry to meet this higher energy demand and a lower NPQ was predicted. The reduced photorespiratory rate at elevated CO_2 also resulted in a reduced ammonia reassimilation flux and the associated energy demand. The HL-E model also predicted a higher starch accumulation rate in agreement with experimental observations (discussed earlier), and as daytime vacuolar malate accumulation and citrate remobilization fluxes in the model were constrained to the starch accumulation rate, the HL-E prediction showed an increased contribution of night-time citrate to the TCA cycle, permitting the model to divert more phospho*enol*-pyruvate towards malate biosynthesis via anaplerotic C fixation. This reduced the predicted flux through PDH in HL-E compared with HL. The complete set of flux predictions for LL, ML, HL, and HL-E conditions is provided in Data S5.

Metabolism in mature and growing leaves

The predictive power of the TC-ODE-FBA model was explored further by comparing the metabolism of fully expanded mature leaves and growing leaves grown at 1000 μmol m^{-2} sec^{-1} photosynthetic photon flux density (PPFD) and 400 ppm CO_2. A complete list of the predicted reaction and transport fluxes in mature and growing leaves is given in Data S6. In total, fluxes were predicted for 728 metabolic reactions and transport steps in mature leaves and 837 in growing leaves. A simplified representation of the major fluxes in mature and growing leaves during the day and night is shown in Figure 7. A comparison between the predicted flux distributions for the two leaf types shows that the dominant daytime fluxes were photosynthetic electron transport and ATP synthesis, and the Calvin cycle and photorespiration. These fluxes were essentially identical in the two leaf types, as would be expected given that these photosynthetic fluxes are primarily determined by the invariant light flux and atmospheric CO_2 concentration. Other fluxes in the wider metabolic network also showed some similarities, most notably a non-cyclic TCA flux, which is consistent with ^{13}C labelling results (Xu et al., 2021).

However, there were also notable differences in the predicted flux distributions between the two leaf types. Mature leaves used assimilated carbon to export sugars and amino acids to the phloem while growing leaves used assimilated carbon to meet the requirement for synthesis of new biomass components (Figure 7). As a result, during the day, there were higher rates of N uptake, amino acid biosynthesis and anaplerotic C-fixation in the growing leaf model to meet the protein demand for growth. The growing leaf model also predicted higher rates of mitochondrial ATP synthesis, primarily to support additional protein synthesis (Figure 7a,b). This is also evident from the ATP budgets calculated from the predicted flux distributions in the mature and growing leaf models (Table 2). In the growing leaf

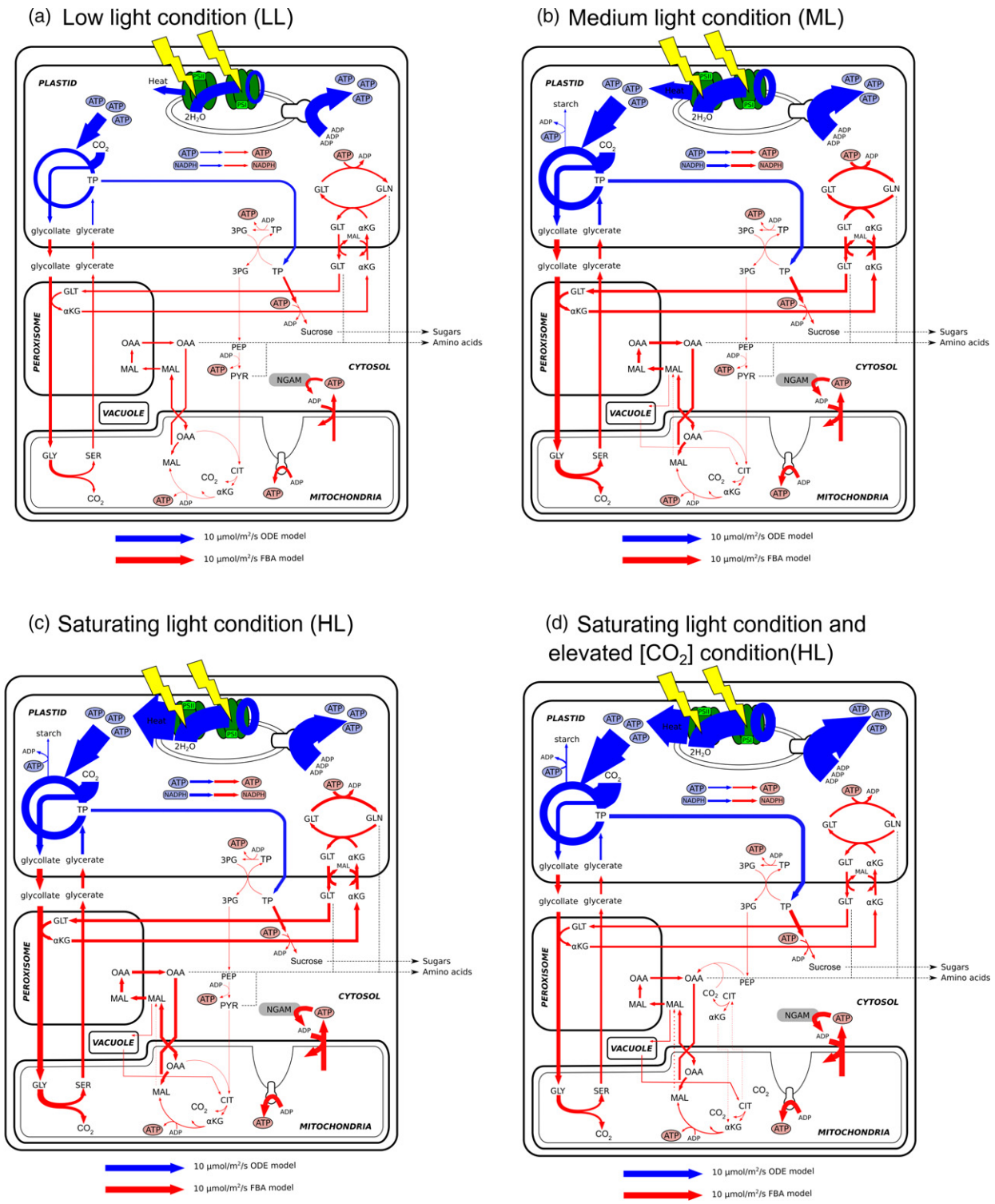

Figure 6. Tightly coupled (TC) ordinary differential equation (ODE)–flux balance analysis (FBA) model can be used to predict metabolic network fluxes under different light intensities and [CO_2] conditions.
The TC-ODE-FBA model was set up for (a) low light (300 μmol photons m^{-2} sec^{-1}, 400 ppm [CO_2]), (b) medium light (600 μmol photons m^{-2} sec^{-1}, 400 ppm [CO_2]), (c) saturating light (1000 μmol photons m^{-2} sec^{-1}, 400 ppm [CO_2]) and (d) saturating light under elevated [CO_2] (1000 μmol photons m^{-2} sec^{-1}, 800 ppm [CO_2]) conditions. In the TC configuration, the ODE model predicts chloroplast metabolism (fluxes in blue) and provides precursors for the FBA model to model fluxes in other compartments and chloroplast metabolic pathways outside the scope of the ODE model (fluxes in red). For clarity only fluxes above a threshold of 0.3 μmol m^{-2} sec^{-1} are depicted. Arrow thicknesses are proportional to flux values. 3PG, 3-phosphoglycerate; CIT, citrate; GLN, glutamine; GLT, glutamate; MAL, malate; NGAM, non-growth associated maintenance; OAA, oxaloacetate; PEP, phospho*enol*pyruvate; PYR, pyruvate; TP, glyceraldehyde 3-phosphate; αKG, 2-oxoglutarate.

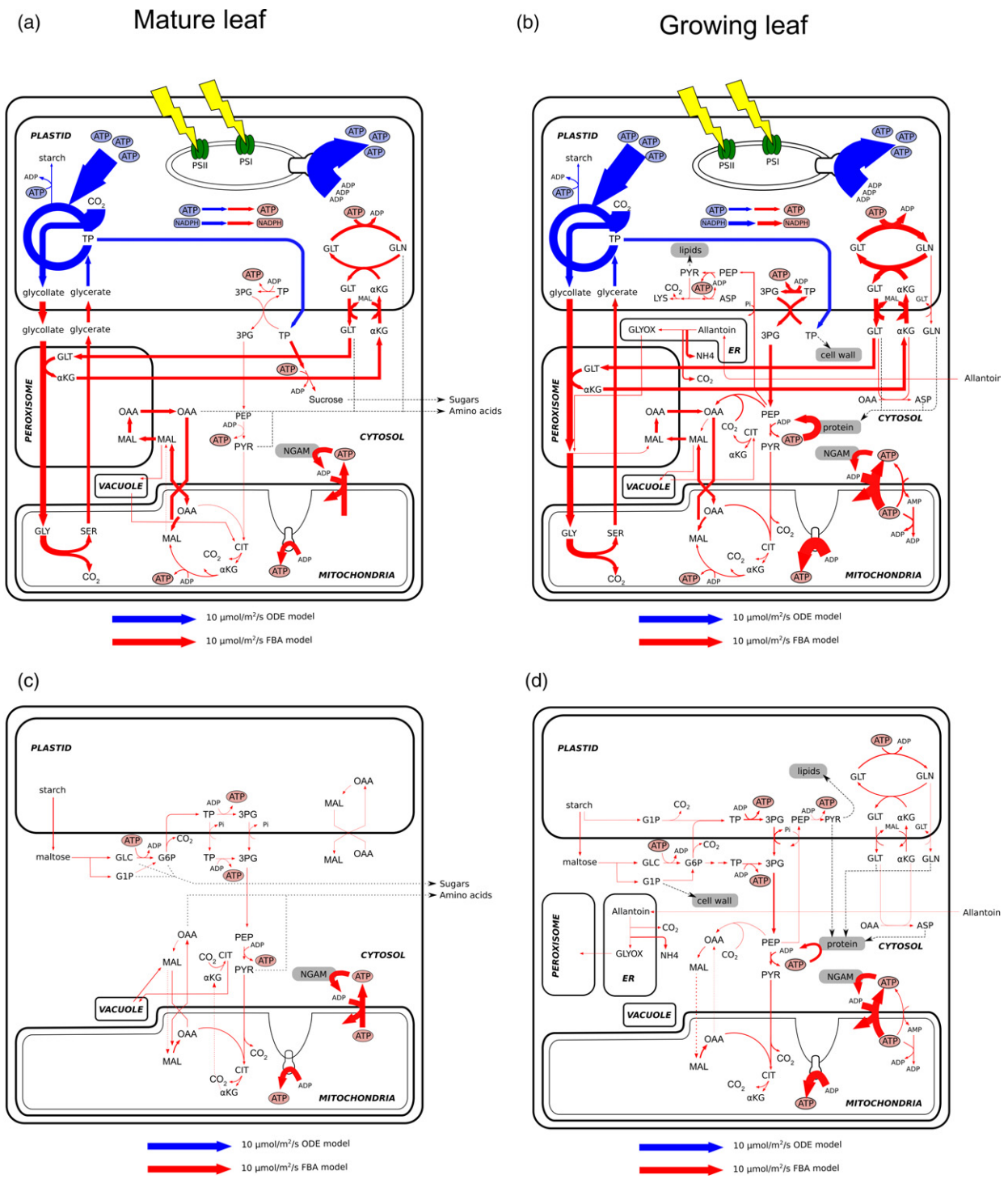

Figure 7. Tightly coupled (TC) ordinary differential equation (ODE)–flux balance analysis (FBA) model can be used to predict metabolic network fluxes in mature and growing leaves in the light and the dark.

The TC-ODE-FBA model was used to model mature and growing leaves under 1000 µmol m^{-2} sec^{-1} photosynthetic photon flux density and 400 ppm [CO_2]. In the TC configuration, the ODE model predicts chloroplast metabolism (fluxes in blue) and provides precursors for the FBA model to model fluxes in other compartments and chloroplast metabolic pathways outside the scope of the ODE model (fluxes in red). The FBA model was configured to model mature leaves exporting sucrose to the phloem during the day (a) and night (c) or growing leaves synthesizing and accumulating biomass during the day (b) and night (d). For clarity only fluxes above a threshold of 0.3 µmol m^{-2} sec^{-1} are depicted. Arrow thicknesses are proportional to flux values. 3PG, 3-phosphoglycerate; ASP, aspartate; CIT, citrate; G1P, glucose 1-phosphate; G6P, glucose 6-phosphate; GLC, glucose; GLN, glutamine; GLT, glutamate; GLY, glycine; GLYOX, glyoxylate; LYS, lysine; MAL, malate; NGAM, non-growth associated maintenance; OAA, oxaloacetate; PEP, phospho*enol*pyruvate; Pi, inorganic phosphate; PYR, pyruvate; SER, serine; TP, glyceraldehyde 3-phosphate; αKG, 2-oxoglutarate.

Table 2 ATP production and consumption in the tightly coupled ODE-FBA model during the day

Metabolic process	ATP flux (μmol m^{-2} sec^{-1})	
	Mature	Growing
Chloroplast ATP synthesis	116.50	116.61
Mitochondrial ATP synthesis	7.24	17.91
Glycolysis	1.19	7.28
Succinyl CoA synthase	1.12	1.22
Structural carbohydrate	0.00	–0.13
Amino acid biosynthesis	–0.04	–1.32
Sucrose synthesis	–1.04	0.00
Starch biosynthesis	–1.33	–1.33
Photorespiration	–4.67	–4.67
GS-GOGAT	–4.83	–8.51
Maintenance	–7.69	–7.69
Protein biosynthesis	0	–12.86
Calvin–Benson cycle	–106.42	–106.43

FBA, flux balance analysis; ODE, ordinary differential equation.
Leaf metabolic fluxes for PPFD = 1000 μmol m^{-2} sec^{-1} and [CO_2] =400 ppm were predicted by the tightly coupled ODE-FBA model. Reaction fluxes involving the consumption and production of ATP from both model components, represented by negative and positive ATP flux values respectively, were used to tabulate ATP consumption and production.

model, fluxes were also observed in reactions associated with the biosynthesis of cellulose, xylan, phosphatidate, palmitoyl acyl carrier protein (ACP), palmitoleoyl ACP, stearoyl ACP, oleoyl ACP, octadecadienoyl ACP, arachidoyl ACP, eicosenoyld ACP, and behenoyl ACP. These fluxes were relatively small and are not depicted in Figure 7b.

Differences between the two leaf types were also apparent in the predicted flux distributions for nocturnal metabolism (Figure 7c,d). The mature leaf model used carbon and energy generated from starch degradation to generate sucrose and amino acids while the growing leaf model used the same to generate protein, lipids, and cell wall (fluxes representing lipid metabolism, cell wall biosynthesis, and parts of the TCA cycle are not depicted in Figure 7c,d as these fluxes were relatively very small). The growing leaf model also showed higher nocturnal N uptake, amino acid biosynthesis, and anaplerotic C-fixation similar to daytime metabolism. In the case of the growing leaf model, higher nocturnal fluxes were also apparent in glycolysis, the TCA cycle and the mitochondrial electron transport chain (Figure 7d) to support the energy demand involved in the synthesis of biomass components.

DISCUSSION

Tight coupling provides a better hybrid ODE-FBA model

The LC-ODE-FBA configuration is the simplest way to integrate ODE and FBA leaf models and it is similar to the individual FBA runs in previous dFBA models (Grafahrend-Belau et al., 2013; Shaw and Cheung, 2018). In this set-up both model elements need to be run only once and hence computation is fast and can be run independently on different platforms with only minimal information being passed from the ODE model to the FBA model. In addition, the FBA component of the LC-ODE-FBA configuration is a diel leaf FBA model and hence this configuration inherits all the advantages of diel leaf FBA models, such as the ability to predict day/night amino acid and organic acid accumulation rates (Cheung et al., 2014). While it has its advantages, the LC-ODE-FBA model also has a major limitation. Kinetic equations based on metabolite and enzyme concentration and reaction kinetics determine the fate of photoassimilates in the ODE model. This part of the ODE model is ignored in the LC-ODE-FBA model, and so while the assimilation rate was predicted accurately, photoassimilate partitioning prediction was inaccurate (Figure 4).

In contrast, the TC-ODE-FBA model accurately predicted both assimilation rate and photoassimilate partitioning. It achieves this by using the ODE model to predict chloroplastic fluxes and then using the FBA model to predict fluxes outside the scope of the ODE model, while allowing the FBA model to relay its chloroplastic energy demand back to the ODE model via the v_{ATP_FBA} and v_{NADPH_FBA} fluxes. These fluxes are fed into the ODE model as steady-state ATP and NADPH sinks, respectively, as they represent the demands of the steady-state FBA model. Under all scenarios modelled here, the ODE model was able to accommodate the constant v_{ATP_FBA} and v_{NADPH_FBA} sinks. However, very large v_{ATP_FBA} and v_{NADPH_FBA} sink fluxes could potentially prevent the ODE model from achieving a feasible solution (by quickly bringing the NADPH or ATP concentration below zero). The likelihood of this was observed to be higher in energy-limited scenarios such as extremely LL and LL at elevated [CO_2]. One possible workaround for this issue is to gradually increase the v_{ATP_FBA} and v_{NADPH_FBA} sink fluxes from 0 to its actual value once the model has been able to achieve a temporary steady state. It should be noted that under extreme energy-limited conditions, the e-photosynthesis model is unable to achieve steady state even in isolation (equivalent to v_{ATP_FBA} and v_{NADPH_FBA} fluxes set to 0). More work on the ODE model is required to overcome this issue. Nevertheless, with this configuration, the TC-ODE-FBA model was able to model leaf metabolism for all conditions discussed in this study, and the results show that the ODE and FBA components complemented each other, thus overcoming many of their individual limitations.

Although both modules needed to be run multiple times in a loop on the same platform, the TC-ODE-FBA model offers a much higher predictive power compared with the LC-ODE-FBA model. In addition, parameter sensitivity analysis showed that the principal predictions (i.e. higher assimilation, starch accumulation, and night-time

respiration rates at higher [CO_2]) held true for ±50% variation in any modelling parameter, as long as a steady state was achievable. It should, however, be noted that the parameter values were assumed to be the same in both ambient and elevated CO_2 conditions here, which may be the case for many kinetic parameters, but non-kinetic parameters such as NGAM costs and organic acid, starch accumulation/remobilization rate ratios are likely to be different under different environmental conditions.

Another significant advantage of TC-ODE-FBA over LC-ODE-FBA is its ability to predict the dissipation of excess light energy. The TC-ODE-FBA analysis of LL, ML, and HL conditions showed energy dissipation increasing with light intensity (Figure 6a–c) (Nicol et al., 2019; Rahimzadeh-Bajgiran et al., 2017). The model also predicted a decrease in NPQ in leaves under HL when atmospheric [CO_2] increased (Figure 6c,d), which has also been previously established in tobacco (Dahal and Vanlerberghe,2018; Miyake et al., 2005). While the model can make many qualitative predictions about the dissipation of excess energy, it still has limitations. As alternative oxidase falls under the FBA component, its contribution to the dissipation of excess energy is not considered in the current TC-ODE-FBA set up. As a result, the model is unable to explore the role of alternative oxidase in the light-stress response (Dahal and Vanlerberghe, 2018). It should be noted that a detailed quantitative assessment of the TC-ODE-FBA model predictions was not possible because of the lack of soybean-specific data. Comparison of the predicted steady-state metabolite concentrations and organic acid stores against experimental data could help identify additional strengths and weaknesses in the model.

While both models have their advantages and disadvantages, it should be noted that in both LC-ODE-FBA and TC-ODE-FBA set-ups, as the FBA and ODE modules were run separately, the linear and non-linear components of the final models are solved separately. As a result, these models can be solved considerably faster than fully integrated hybrid models, such as the one described by Pozo et al. (2015), where the linear and non-linear components have to be solved together as a single non-linear problem. As such the couplings facilitated by integration tools such as yggdrasil provide a significant improvement over previously published models of leaf metabolism.

TC-ODE-FBA model provides a comprehensive description of leaf metabolism

Nocturnal respiration has a significant bearing on the overall change to crop productivity and contradictory data about respiratory responses to high [CO_2] has been reported (Davey et al., 2004; Drake et al., 1999). Both ODE and FBA models on their own are unable to explore such respiratory responses. However, the TC-ODE-FBA model is capable of modelling night-time metabolism under different atmospheric [CO_2] and the interaction of night-time respiration with changes in daytime photosynthesis and non-structural carbohydrate levels. The TC-ODE-FBA successfully predicted the increased transitory starch storage and higher night-time respiration with growth under elevated [CO_2]. It provides a theoretical underpinning to the controversial observation of increased, rather than decreased, night-time respiration observed in plants grown under elevated [CO_2] of Davey et al., (2004). The predicted increase in transitory starch stores in leaves grown in elevated CO_2 also agrees with previous experimental observations (Ainsworth et al., 2007; Grimmer et al., 1999; Rogers et al., 2004). As the FBA model representing night-time metabolism then remobilizes all the transitory starch a higher respiration rate is observed (Figure 6). While this increased rate of night-time respiration is in agreement with published data (Davey et al., 2004), it should be noted that the assumption that all of the transitory starch is remobilized may not always be the case. Grimmer et al. (1999) reported that castor bean leaves grown in elevated [CO_2] only partially use up the available starch pool. However, data from soy grown using FACE suggests that the leaves are able to use the entire starch pool (Rogers et al., 2004) thus supporting the assumption in the FBA model. Closer inspection of the nocturnal fluxes involving CO_2 in mature leaves showed that while the oxidative PPP and PDH are responsible for most of the CO_2 respired, the contributions from the TCA cycle, malic enzyme, and amino acid biosynthesis were also significant (Table 1).

One of the key features of the TC-ODE-FBA model is its ability to use fluxes from the ODE model to predict fluxes through several hundred reactions with relatively little experimental data. Soy-specific gas exchange data were used to parameterize the ODE component. The FBA component of the model required petiole phloem composition (when modelling mature leaves) and leaf biomass composition (when modelling growing leaves). Soy-specific petiole phloem composition data were not available and hence data from tomatoes available from the literature were used instead (Table S6). Although a quite different species, sensitivity analysis showed that varying phloem composition had negligible impact on the quantitative results discussed in this study (Table S5). Soy leaf biomass composition required to model growing soy leaves was experimentally determined (Table S7).

To highlight the utility of the model, we also used the TC-ODE-FBA model to compare metabolic fluxes in fully expanded mature leaves and growing leaves. While Figure 7 was used to highlight the differences between the two different modelling scenarios, many differences could not be depicted in Figure 7 owing to these pathways carrying very small fluxes. An example of this is lipid biosynthesis. The TC-ODE-FBA model predicted growing leaves to

synthesize phosphatidate at a rate of 2.47×10^{-18} μmol m^{-2} sec^{-1} during the day (Data S6). In other cases, similarities existed between the two scenarios that were not depicted in Figure 7, such as when pathways in the TC-ODE-FBA model did not carry any flux. An example of one such a pathway is fatty acid degradation. While fatty acid turnover is likely active in both mature and growing leaves, FBA is incapable of capturing this and hence does not predict fluxes through these pathways. This is also the reason why the mature leaf flux distribution did not predict any lipid biosynthesis. Analysis also showed that the TC-ODE-FBA model predicted a non-cyclic TCA flux in both mature and growing leaves. In both systems, mitochondrial MDH operated in the reverse direction to the conventional TCA cycle, generating malate, which is in agreement with stable isotope labelling studies (Ma et al., 2014; Tcherkez et al., 2009; Xu et al., 2021). This is because photorespiratory flux generates a significant amount of NADH in the mitochondria, which has to be shuttled out into the cytosol via the malate valve (Shameer et al., 2019).

Among the many differences between the two metabolic systems, a significantly higher PEPC activity was predicted in growing leaves. PEPC activity results in the generation of oxaloacetate, which can be either reduced to malate, transaminated to aspartate or converted to citrate and then 2-oxoglutarate via the TCA cycle. Growing leaves have a higher protein demand compared with mature leaves and as a result they exhibit increased allantoin uptake and amino acid biosynthesis (Figure 7). An increased rate of amino acid biosynthesis would generate higher oxaloacetate demands in the system. Anaplerotic C fixation can generate oxaloacetate required for aspartate biosynthesis and this association between PEPC activity and aspartate levels has been previously discussed (Tcherkez and Hodges, 2008). In addition, aspartate is also the precursor for lysine, isoleucine, and methionine and so the TC-ODE-FBA model predicted increased anaplerotic C fixation in growing leaves. While there is no direct evidence to support this, evidence for positive correlation between N uptake rate and PEPC activity has been reported (Scheible et al., 1997). Besides increased oxaloacetate demands, an increased rate of amino acid biosynthesis would result in increased 2-oxoglutarate demands. Isotopic labelling (^{13}C) studies in leaves have shown that the majority of daytime 2-oxoglutarate is generated from metabolites accumulated during the previous night (Gauthier et al., 2010). While 2-oxoglutarate can be generated from citrate stores, it has been shown that this citrate alone is insufficient to meet the leaf's 2-oxoglutarate demands (Tcherkez et al., 2017). Vacuolar aspartate (accumulated during the previous night) has also been proposed as a potential precursor of 2-oxoglutarate and glutamate (Gauthier et al., 2010). However, this also points towards a higher night-time PEPC flux under higher daytime amino acid demand, as the TC-ODE-FBA model (in its current state) was constrained not to accumulate amino acids during the day. Enabling the TC-ODE-FBA model to accumulate additional metabolites in the vacuole such as sugars and amino acids would potentially improve the ability of this model to capture such complex flux distributions, although with the trade-off of a greater solution space and the potential for non-realistic flux cycling between day and night.

Future development of hybrid ODE-FBA models

There are many challenges involved in developing hybrid ODE-FBA models (Marshall-Colon et al., 2017). While challenges such as identifying connection points or adjusting for the difference in time scales between models are case-specific, technical challenges such as the difficulty of coupling models running on different platforms and transferring information between models can now be generalized and solved efficiently using cross-platform model integration frameworks such as yggdrasil (Lang, 2019). While model run-time issues are partly case-specific, the choice for integration framework or platform could help speed up model runs. Yggdrasil uses a Python-based environment to execute the individual models, even those native to other platforms, and passes information between them. The availability of fast ODE solvers in MATLAB makes it a good choice to run ODE models. Yggdrasil runs such models, such as the e-photosynthesis ODE model, by launching the MATLAB engine via Python. This process is somewhat time-consuming and was noted to slow down both LC and TC models by 10–20%. Nevertheless, yggdrasil simplifies the process of developing tailored hybrid models, so much so that there is now a strong incentive to enhance FBA models with relevant ODE models and vice-versa.

This study shows how metabolic modelling of C_3 leaves is improved by coupling ODE and FBA models. Similar advantages of coupling ODE and FBA models are yet to be explored in other plant metabolic systems. As in the case of C_3 photosynthesis described here, kinetic models of C_4 photosynthesis also lack representations for many pathways in primary metabolism (Wang et al., 2014). Coupling such models to FBA models of C_4 leaves (Bogart and Myers, 2016; de Oliveira Dal'Molin et al., 2010) should lead to an improved representation of C_4 metabolism. Storage organs provide another example of a metabolic system, which could be better described by tailored hybrid models such as the one described here. FBA models are unable to predict fluxes through futile cycles, an important contributor to metabolic regulation (Claeyssen et al., 2013). ODE models have been shown to be capable of predicting the futile cycling of sucrose in sugarcane (Rohwer and Botha 2001; Uys et al 2007). Further ODE-FBA coupling hence has the potential to help the FBA model improve the quality of its predictions by accounting for futile cycles, all the while

modelling fluxes through metabolic pathways outside the scope of the ODE models. While ODE-based photosynthesis models and diel FBA leaf models have helped improve our understanding of leaf metabolism and have contributed to the development of ideas for metabolic manipulations (Cheung et al., 2014; Shameer et al., 2018; Wang et al., 2014; Zhu et al., 2007,), the higher predictive power and metabolic coverage of the TC model has the potential to improve further upon these ideas and additional applications as illustrated here.

EXPERIMENTAL PROCEDURES

Plant materials and growth conditions

Mature leaf tissue samples from soybean plants (*Glycine max* cv. P29A85L) grown at the SoyFACE facility on the South Farms of the University of Illinois, Champaign, IL, USA (www.igb.illinois.edu/soyface/, 40°02′N, 88°14′W) were collected on 9 August 2019. Samples were collected from plants grown in four ambient CO_2 (410 ppm) and four elevated CO_2 plots (600 ppm) into liquid N_2. Leaf tissue was freeze-dried, powdered, and kept at −80°C until analysed.

Leaf biomass measurements

Total cell wall and total lipid were analysed by weight following selective extraction according to Poolman et al., 2009. Starch was assayed by enzymatic digestion according to Smith and Zeeman (2006), except that the tissue was extracted in methanol–chloroform and the released glucose was analysed by gas chromatography–mass spectrometry (GC-MS) following Lisec et al. (2006). The insoluble material following starch digestion was used for the determination of cell wall sugar composition as follows: the insoluble material was washed twice with 70% (v/v) ethanol and then incubated with 2 M trifluoracetic acid at 120°C for 1 h to hydrolyse the cell wall to component sugars that were recovered, derivatized, and quantified by GC-MS (Lisec et al., 2006). The amino acid content of total protein was determined by selective extraction of total protein, acid hydrolysis, and quantification of released amino acids by GC-MS according to Long and Antoniewicz (2014). The fatty acid content of lipids was analysed by solvent extraction of total lipid, esterification to produce fatty acid methyl esters and quantification of fatty acid methyl esters by GC-MS according to Laurens et al. (2012). Soluble metabolite profiles were obtained by GC-MS analysis of methanol–chloroform extracts according to Lisec et al. (2006).

ODE leaf model

The e-photosynthesis model (Zhu et al., 2013) is an ODE-based metabolic model of C_3 photosynthesis encoded in MATLAB. This model was built as a generic C_3 photosynthesis model and was not parameterized for any specific species but built from averages across species where individual kinetic parameters had been determined experimentally. To simulate the photosynthetic rate of soybean under various CO_2 conditions, the estimated CO_2 uptake rate of the e-photosynthesis ODE model was calibrated using measured gas exchange data for soybean leaves (Bernacchi et al., 2005). The calibration was achieved by adjusting the maximum enzyme activity of RuBisCo ($V_{m\_Rubisco}$) in the e-photosynthesis model so that the simulated maximum activity of RuBisCo (V_{cmax_s}) was equal to the measured V_{cmax} of soybean (Bernacchi et al., 2005). This required $V_{m\_Rubisco}$ to be increased to 1.33 times that of the value used in the original e-photosynthesis model ($V_{m\_Rubisco\_o}$) (Figure S2). Maximum activities of other Calvin–Benson Cycle and starch synthesis enzymes (V_{m_E}) were also linearly transformed so that the simulated maximum RuBP regeneration rate (J_{max_s}) was equal to the measured maximum RuBP regeneration rate (J_{max}) of soybean (Bernacchi et al., 2005). This required V_{m_E} to be increased to 1.36 times the value used in the original e-photosynthesis model ($V_{m\_E\_o}$) (Figure S2). Calibrating the model in this manner was found to achieve the purpose of fitting the model to soybean V_{cmax} and J_{max} data with the least number of parameters introduced into the model. Thus, the calibrated maximum rates of the photosynthetic enzyme activities were:

$$V_{m\_Rubisco} = V_{m\_Rubisco\_o} \cdot \alpha_{Rubisco} \quad (5)$$

$$V_{m\_E} = V_{m\_E\_o} \cdot \alpha_E \quad (6)$$

where $\alpha_{Rubisco}$ is 1.33 and α_E is 1.36 (Figure S1). Adjusted parameters for these enzymes are listed in Table S8. All other parameters were the same as those used in the original e-photosynthesis model (Zhu et al., 2013). Finally, to avoid unreasonable results, constraints were added to ensure reaction rates of glyceraldehyde-3-phosphate dehydrogenase and starch degradation were always non-negative.

For each simulation of the kinetic model, the slope of the change of CO_2 assimilation rate with time and each metabolite concentration was checked to evaluate whether the model had reached a steady state.

FBA leaf model

An updated version (v2.0.0, model curation log presented in Data S7) of the previously published charge and proton-balanced PLANTCOREMETABOLISM model (Shameer et al., 2020) was used in this study to generate FBA models. *Glycine max* specific gene–protein–reaction associations were gathered from the PlantCyc Soy Pathway/Genome Database (PGDB) (https://www.plantcyc.org/). Data from the cropPAL database (Hooper et al., 2016) was used to ensure gene–protein–reaction associations were in line with known enzyme subcellular localization. The purpose of mature leaves in higher plants is to use light energy via photosynthesis to generate carbon skeletons and undertake metabolism to load the phloem sap with sugars, amino acids, and organic acids for the rest of the plant. Owing to the lack of soybean-specific data on petiole phloem sap composition, previously published data from tomatoes (Valle et al., 1998; Walker and Ho, 1977) was used to generate the reaction representing the export of sugars and amino acids into phloem from mature leaves in prescribed proportions (Table S6). As a nodulating legume, allantoin is considered the major leaf nitrogen source (Fujihara et al., 1977). To model this aspect of metabolism, the allantoin catabolism pathway was added to the model from the PlantCyc Soy PGDB. The four hydrolases involved in breaking down allantoin to glyoxylate releasing four moles of NH_4^+ and two moles of CO_2, were assumed to be endoplasmic reticulum localized based on annotations of the genes associated on UniProt and findings from Arabidopsis (Takagi et al., 2018). Allantoin uptake into the leaf was assumed to be facilitated via the ENT3 transporter (Niño-González et al., 2019), which has been reported to utilize a proton-symport mechanism (Traub et al., 2007). The charge states of all added metabolites were predicted using MARVINSKETCH 21.9.0 (https://www.chemaxon.com) and all added reactions were charged and proton balanced as previously (Shameer et al., 2018). An SBML version of the soy-specific version of PLANTCOREMETABOLISM v2.0.0 used in the study is available in Data S8.

A diel leaf FBA model was generated from the soy-specific version of the PLANTCOREMETABOLISM model using the method described

elsewhere (Cheung et al., 2014; Shameer et al., 2019). This entailed duplicating all model elements (compartments, reactions, and metabolites) to represent daytime and night-time metabolism and adding 'linker' reactions (reactions that convert daytime metabolites to their respective night-time metabolites and vice versa, to represent diel metabolite accumulation and consumption). Linker reactions were included for chloroplast starch, vacuolar sucrose, vacuolar organic acids, and vacuolar amino acids. A complete list of all constraints used to set-up the diel leaf FBA model is presented in Table S9. To model mature leaves, pFBA was used to model fluxes through the metabolic network maximizing the export of sucrose and amino acids from the leaf.

Modelling metabolism of mature soybean leaves across a range of light intensities and atmospheric CO_2 concentrations

The two original models (ODE leaf model, the diel FBA leaf model) and the two hybrid models (LC-ODE-FBA and TC-ODE-FBA) were used to model the assimilation rate (*A*) in leaves experiencing a range of light intensities and atmospheric CO_2 concentrations (*Ca*) The resulting assimilation rates were used to generate *A*-*Ci* and *A*-PPFD curves for each model, based on the assumption that $Ci = 0.7 \times Ca$, where *Ci* is the intercellular [CO_2] (Ainsworth and Long, 2005; Long et al., 2004). Previously published data on assimilation rates observed under different intercellular [CO_2] and HL intensities (Morgan et al., 2004; Sun et al., 2014) and assimilation rates observed under different light intensities and ambient [CO_2] (Haile and Higley, 2003; Yao et al., 2017; Zhang et al., 2011) were used to evaluate the accuracy of the model predictions.

Modelling metabolism of mature soybean leaves from plants grown in FACE experiments

Records of diurnal variations of canopy incident light intensity for soybean in ambient [CO_2] and [CO_2] elevated to 550 μmol mol^{-1} under open air conditions using FACE technology over the growing season (Rogers et al., 2004) were collected. Hourly light intensities during the experiment were estimated by linear interpolation. Daytime leaf metabolism for each hour of the photoperiod was modelled using the ODE, FBA, LC-ODE-FBA and TC-ODE-FBA set-ups, and CO_2 assimilation, PSII electron flux and starch accumulation rates were recorded. Leaf starch content at noon predicted by each model was calculated by adding up all hourly starch accumulation rate predictions from dawn to noon. Night-time metabolism in the TC-ODE-FBA model driven by total starch accumulated during the photoperiod, accounting for changes in day-length over the growing season, was modelled using the FBA model as described earlier.

Modelling metabolism in mature and growing soybean leaves

The TC-ODE-FBA model was used to compare the metabolism of mature and growing soybean leaves at 400 μmol mol^{-1} atmospheric [CO_2] and 1000 μmol m^{-2} sec^{-1} PPFD. Mature leaves were modelled using TC-ODE-FBA with an objective function to maximize the export of sucrose and amino acids into the phloem using pFBA. To model growing leaves, the biomass composition of soy leaf was experimentally determined (Table S7) and a biomass reaction representing the accumulation of biomass elements in the observed ratios was added to the FBA model. The growing leaf was then modelled by optimizing the flux distribution to maximize flux through the biomass reaction using pFBA during the FBA runs of the TC-ODE-FBA model.

Model execution

The ODE model was executed on MATLAB 2020a using its ODE15s solver. All FBA models were run on Python 3.7.6 using the cobrapy v0.17.1 package and the default GLPK solver. Yggdrasil was used to coordinate the execution of the two models in their native environments and the transfer of information between them.

ACKNOWLEDGMENTS

Research reported in the publication was supported by the Foundation for Food and Agriculture Research under award number – Grant ID: 602757. The content of this publication is solely the responsibility of the authors and does not necessarily represent the official views of the Foundation for Food and Agriculture Research.

AUTHOR CONTRIBUTIONS

RGR, SPL, and LJS supervised this study; YW collected all biological samples; PB carried out all leaf biomass measurements; SS, YW, RGR, SPL, and LJS developed the hybrid models. SS and YW performed the modelling and analysed the results; SS, YW, RGR, SPL, and LJS wrote the article; all authors approved the final version of the article for publication.

CONFLICT OF INTERESTS

The authors declare that they have no competing interests.

DATA AVAILABILITY STATEMENT

All models, MATLAB scripts, Python scripts, yggdrasil YAML files and input files required to run the FBA model, ODE model, LC and TC models are available in the github repository: https://github.com/cropsinsilico/ODE_FBA_Photosynthesis2021. All other relevant data can be found within the manuscript and its supporting materials.

SUPPORTING INFORMATION

Additional Supporting Information may be found in the online version of this article.

Data S1. Flux distribution for FACE conditions predicted by the ODE model.

Data S2. Flux distribution for FACE conditions predicted by the TC-ODE-FBA model.

Data S3. Flux distribution for FACE conditions predicted by the LC-ODE-FBA model.

Data S4. Flux distribution for FACE conditions predicted by the FBA model.

Data S5. Daytime flux distributions for LL, ML, HL, and HL-E conditions predicted by the TC-ODE-FBA model.

Data S6. Flux distribution in mature and growing leaves predicted by the TC-ODE-FBA model.

Data S7. Updates to PLANTCOREMETABOLISM v1.2.0.

Data S8. SBML file of soy-specific PLANTCOREMETABOLISM v2.0.0.

Figure S1. Models in tightly coupled configuration achieve convergence within a small number of cycles.

Figure S2. Estimated V_{cmax_S} and J_{max_S} from A-Ci curves generated by e-photosynthesis model.

Information S1. Evaluating the sensitivity of tightly coupled ODE-FBA model (TC-ODE-FBA) results to model parameters.

Table S1. Relationship between malate and citrate accumulation or remobilization fluxes and starch accumulation flux in the diel FBA model.

Table S2. Metabolic constraints for the single phase daytime model.

Table S3. Metabolic constraints for the single phase night-time model.

Table S4. A comparison of the capabilities of the ODE, FBA, LC-ODE-FBA, and TC-ODE-FBA models.

Table S5. Sensitivity analysis of the TC-ODE-FBA model parameters.

Table S6. Phloem composition gathered from previously published studies.

Table S7. Soy leaf biomass composition.

Table S8. Adjusted maximum enzyme activities (V_{max}) in the e-photosynthesis model.

Table S9. Metabolic constraints for the diel leaf model.

REFERENCES

Ainsworth, E.A. & Long, S.P. (2005) What have we learned from 15 years of free-air CO_2 enrichment (FACE)? A meta-analytic review of the responses of photosynthesis, canopy properties and plant production to rising CO_2. *New Phytologist*, **165**, 351–372.

Ainsworth, E.A., Rogers, A., Leakey, A.D., Heady, L.E., Gibon, Y., Stitt, M. *et al.* (2007) Does elevated atmospheric [CO2] alter diurnal C uptake and the balance of C and N metabolites in growing and fully expanded soybean leaves? *Journal of Experimental Botany*, **58**, 579–591.

Arnold, A. & Nikoloski, Z. (2014) Bottom-up metabolic reconstruction of Arabidopsis and its application to determining the metabolic costs of enzyme production. *Plant Physiology*, **165**, 1380–1391.

Beard, D.A. & Qian, H. (2005) Constraint-based modeling of metabolomic systems. In *Encyclopedia of Genetics, Genomics, Proteomics, Bioinformatics* (Jorde, L.B., Little, P.F.R., Dunn, M.J. & Subramaniam, S. eds). Chichester: John Wiley, Sons Ltd, p. 3.

Bernacchi, C.J., Morgan, P.B., Ort, D.R. & Long, S.P. (2005) The growth of soybean under free air [CO_2] enrichment (FACE) stimulates photosynthesis while decreasing *in vivo* Rubisco capacity. *Planta*, **220**, 434–446.

Bogart, E. & Myers, C.R. (2016) Multiscale metabolic modeling of C4 plants: connecting nonlinear genome-scale models to leaf-scale metabolism in developing maize leaves. *PLoS One*, **11**, e0151722.

Chatterjee, A., Huma, B., Shaw, R. & Kundu, S. (2017) Reconstruction of *Oryza sativa indica* genome scale metabolic model and its responses to varying rubisco activity, light intensity, and enzymatic cost conditions. *Frontiers in Plant Science*, **8**, 2060.

Cheung, C.M., Poolman, M.G., Fell, D.A., Ratcliffe, R.G. & Sweetlove, L.J. (2014) A diel flux balance model captures interactions between light and dark metabolism during day-night cycles in C_3 and crassulacean acid metabolism leaves. *Plant Physiology*, **165**, 917–929.

Cheung, C.M., Ratcliffe, R.G. & Sweetlove, L.J. (2015) A method of accounting for enzyme costs in flux balance analysis reveals alternative pathways and metabolite stores in an illuminated Arabidopsis leaf. *Plant Physiology*, **169**, 1671–1682.

Claeyssen, É., Dorion, S., Clendenning, A., He, J.Z., Wally, O., Chen, J. *et al.* (2013) The futile cycling of hexose phosphates could account for the fact that hexokinase exerts a high control on glucose phosphorylation but not on glycolytic rate in transgenic potato (*Solanum tuberosum*) roots. *PLoS One*, **8**, e53898.

Cox, P., Betts, R., Bunton, C., Essery, R., Rowntree, P. & Smith, J. (1999) The impact of new land surface physics on the GCM simulation of climate and climate sensitivity. *Climate Dynamics*, **15**, 183–203.

Dahal, K. & Vanlerberghe, G.C. (2018) Growth at elevated CO_2 requires acclimation of the respiratory chain to support photosynthesis. *Plant Physiology*, **178**, 82–100.

Davey, P.A., Hunt, S., Hymus, G.J., DeLucia, E.H., Drake, B.G., Karnosky, D.F. *et al.* (2004) Respiratory oxygen uptake is not decreased by an instantaneous elevation of [CO_2], but is increased with long-term growth in the field at elevated [CO_2]. *Plant Physiology*, **134**, 520–527.

de Oliveira Dal'Molin, C.G., Quek, L.-E., Palfreyman, R.W., Brumbley, S.M. & Nielsen, L.K. (2010) C4GEM, a genome-scale metabolic model to study C_4 plant metabolism. *Plant Physiology*, **154**, 1871–1885.

de Oliveira Dal'Molin, C.G., Quek, L.-E., Palfreyman, R.W., Brumbley, S.M. & Nielsen, L.K. (2010) AraGEM, a genome-scale reconstruction of the primary metabolic network in Arabidopsis. *Plant Physiology*, **152**, 579–589.

Drake, B.G., Azcon-Bieto, J., Berry, J., Bunce, J., Dijkstra, P., Farrar, J. *et al.* (1999) Does elevated atmospheric CO_2 concentration inhibit mitochondrial respiration in green plants? *Plant, Cell & Environment*, **22**, 649–657.

Farquhar, G.D., von Caemmerer, S. & Berry, J. (1980) A biochemical model of photosynthetic CO_2 assimilation in leaves of C_3 species. *Planta*, **149**, 78–90.

Fridlyand, L.E. & Scheibe, R. (1999) Regulation of the Calvin cycle for CO_2 fixation as an example for general control mechanisms in metabolic cycles. *Biosystems*, **51**, 79–93.

Fujihara, S., Yamamoto, K. & Yamaguchi, M. (1977) A possible role of allantoin and the influence of nodulation on its production in soybean plants. *Plant and Soil*, **48**, 233–242.

Gauthier, P.P.G., Bligny, R., Gout, E., Mahé, A., Nogués, S., Hodges, M. *et al.* (2010) *In folio* isotopic tracing demonstrates that nitrogen assimilation into glutamate is mostly independent from current CO_2 assimilation in illuminated leaves of *Brassica napus*. *New Phytologist*, **185**(4), 988–999.

Gombert, A.K. & Nielsen, J. (2000) Mathematical modelling of metabolism. *Current Opinion in Biotechnology*, **11**, 180–186.

Grafahrend-Belau, E., Junker, A., Eschenröder, A., Müller, J., Schreiber, F. & Junker, B.H. (2013) Multiscale metabolic modeling: dynamic flux balance analysis on a whole-plant scale. *Plant Physiology*, **163**, 637–647.

Grimmer, C., Bachfischer, T. & Komor, E. (1999) Carbohydrate partitioning into starch in leaves of *Ricinus communis* L. grown under elevated CO_2 is controlled by sucrose. *Plant, Cell & Environment*, **22**, 1275–1280.

Haile, F.J. & Higley, L.G. (2003) Changes in soybean gas-exchange after moisture stress and spider mite injury. *Environmental Entomology*, **32**, 433–440.

Heckmann, D., Schulze, S., Denton, A., Gowik, U., Westhoff, P., Weber, A.P. *et al.* (2013) Predicting C_4 photosynthesis evolution: modular, individually adaptive steps on a Mount Fuji fitness landscape. *Cell*, **153**, 1579–1588.

Herrmann, H.A., Dyson, B.C., Vass, L., Johnson, G.N. & Schwartz, J.-M. (2019) Flux sampling is a powerful tool to study metabolism under changing environmental conditions. *NPJ Systems Biology and Applications*, **5**, 32.

Hooper, C.M., Castleden, I.R., Aryamanesh, N., Jacoby, R.P. & Millar, A.H. (2016) Finding the subcellular location of barley, wheat, rice and maize proteins: the compendium of crop proteins with annotated locations (cropPAL). *Plant and Cell Physiology*, **57**, e9(1–9).

Imam, S., Schäuble, S., Valenzuela, J., García, L., de Lomana, A., Carter, W. *et al.* (2015) A refined genome-scale reconstruction of Chlamydomonas metabolism provides a platform for systems-level analyses. *The Plant Journal*, **84**, 1239–1256.

Kamsen, R., Kalapanulak, S., Chiewchankaset, P. & Saithong, T. (2021) Transcriptome integrated metabolic modeling of carbon assimilation underlying storage root development in cassava. *Scientific Reports*, **11**, 8758.

Kleessen, S., Irgang, S., Klie, S., Giavalisco, P. & Nikoloski, Z. (2015) Integration of transcriptomics and metabolomics data specifies the metabolic response of Chlamydomonas to rapamycin treatment. *The Plant Journal*, **81**, 822–835.

Kleessen, S. & Nikoloski, Z. (2012) Dynamic regulatory on/off minimization for biological systems under internal temporal perturbations. *BMC Systems Biology*, **6**, 16.

Kromdijk, J., Głowacka, K., Leonelli, L., Gabilly, S.T., Iwai, M., Niyogi, K.K. *et al.* (2016) Improving photosynthesis and crop productivity by accelerating recovery from photoprotection. *Science*, **354**, 857–861.

Laisk, A., Eichelmann, H., Oja, V., Eatherall, A. & Walker, D.A. (1989) A mathematical model of the carbon metabolism in photosynthesis. Difficulties in explaining oscillations by fructose 2, 6-bisphosphate regulation. *Proceedings of the Royal Society of London. B. Biological Sciences*, **237**, 389–415.

Laisk, A. & Walker, D.A. (1986) Control of phosphate turnover as a rate-limiting factor and possible cause of oscillations in photosynthesis: a

mathematical model. *Proceedings of the Royal society of London. Series B. Biological sciences*, **227**, 281–302.

Lakshmanan, M., Lim, S.-H., Mohanty, B., Kim, J.K., Ha, S.-H. & Lee, D.-Y. (2015) Unraveling the light-specific metabolic and regulatory signatures of rice through combined in silico modeling and multiomics analysis. *Plant Physiology*, **169**, 3002–3020.

Lang, M. (2019) yggdrasil: a Python package for integrating computational models across languages and scales. *Silico Plants*, **1**, diz001.

Laurens, L.M., Quinn, M., Van Wychen, S., Templeton, D.W. & Wolfrum, E.J. (2012) Accurate and reliable quantification of total microalgal fuel potential as fatty acid methyl esters by in situ transesterification. *Analytical and Bioanalytical Chemistry*, **403**, 167–178.

Lisec, J., Schauer, N., Kopka, J., Willmitzer, L. & Fernie, A.R. (2006) Gas chromatography mass spectrometry–based metabolite profiling in plants. *Nature Protocols*, **1**, 387–396.

Long, C.P. & Antoniewicz, M.R. (2014) Quantifying biomass composition by gas chromatography/mass spectrometry. *Analytical Chemistry*, **86**, 9423–9427.

Long, S.P., Ainsworth, E.A., Rogers, A. & Ort, D.R. (2004) Rising atmospheric carbon dioxide: Plants face the future. *Annual Review of Plant Biology*, **55**, 591–628.

Long, S., Burgess, S. & Causton, I. (2019) Redesigning crop photosynthesis. In: Zeigler, R. (Ed.) *Sustaining Global Food Security: The Nexus of Science and Policy*. Canberra: CSIRO Publishing, pp. 61–144.

López-Calcagno, P.E., Brown, K.L., Simkin, A.J., Fisk, S.J., Vialet-Chabrand, S., Lawson, T. *et al.* (2020) Stimulating photosynthetic processes increases productivity and water-use efficiency in the field. *Nature Plants*, **6**, 1054–1063.

Ma, F., Jazmin, L.J., Young, J.D. & Allen, D.K. (2014) Isotopically nonstationary ^{13}C flux analysis of changes in *Arabidopsis thaliana* leaf metabolism due to high light acclimation. *Proceedings of the National Academy of Sciences*, **111**, 16967–16972.

Marshall-Colon, A., Long, S.P., Allen, D.K., Allen, G., Beard, D.A., Benes, B. *et al.* (2017) Crops *in silico*: generating virtual crops using an integrative and multi-scale modeling platform. *Frontiers in Plant Science*, **8**, 786.

McGrath, J.M. & Long, S.P. (2014) Can the cyanobacterial carbon-concentrating mechanism increase photosynthesis in crop species? A theoretical analysis. *Plant Physiology*, **164**, 2247–2261.

Miguez, F.E., Zhu, X., Humphries, S., Bollero, G.A. & Long, S.P. (2009) A semimechanistic model predicting the growth and production of the bioenergy crop *Miscanthus×giganteus*: description, parameterization and validation. *GCB Bioenergy*, **1**, 282–296.

Mintz-Oron, S., Meir, S., Malitsky, S., Ruppin, E., Aharoni, A. & Shlomi, T. (2012) Reconstruction of Arabidopsis metabolic network models accounting for subcellular compartmentalization and tissue-specificity. *Proceedings of the National Academy of Sciences*, **109**, 339–344.

Miyake, C., Miyata, M., Shinzaki, Y. & Tomizawa, K. (2005) CO_2 response of cyclic electron flow around PSI (CEF-PSI) in tobacco leaves—Relative electron fluxes through PSI and PSII determine the magnitude of non-photochemical quenching (NPQ) of Chl fluorescence. *Plant and Cell Physiology*, **46**, 629–637.

Morales, A., Yin, X., Harbinson, J., Driever, S.M., Molenaar, J., Kramer, D.M. *et al.* (2018) In silico analysis of the regulation of the photosynthetic electron transport chain in C_3 plants. *Plant Physiology*, **176**, 1247–1261.

Morgan, P.B., Bernacchi, C.J., Ort, D.R. & Long, S.P. (2004) An in vivo analysis of the effect of season-long open-air elevation of ozone to anticipated 2050 levels on photosynthesis in soybean. *Plant Physiology*, **135**, 2348–2357.

Nicol, L., Nawrocki, W.J. & Croce, R. (2019) Disentangling the sites of non-photochemical quenching in vascular plants. *Nature Plants*, **5**, 1177–1183.

Niño-González, M., Novo-Uzal, E., Richardson, D.N., Barros, P.M. & Duque, P. (2019) More transporters, more substrates: the Arabidopsis major facilitator superfamily revisited. *Molecular Plant*, **12**, 1182–1202.

Orth, J.D., Thiele, I. & Palsson, B.Ø. (2010) What is flux balance analysis? *Nature Biotechnology*, **28**, 245–248.

Paul, M.J. & Foyer, C.H. (2001) Sink regulation of photosynthesis. *Journal of Experimental Botany*, **52**, 1383–1400.

Paul, M.J. & Pellny, T.K. (2003) Carbon metabolite feedback regulation of leaf photosynthesis and development. *Journal of Experimental Botany*, **54**, 539–547.

Pearcy, R., Gross, L. & He, D. (1997) An improved dynamic model of photosynthesis for estimation of carbon gain in sunfleck light regimes. *Plant, Cell & Environment*, **20**, 411–424.

Poolman, M.G., Fell, D.A. & Thomas, S. (2000) Modelling photosynthesis and its control. *Journal of Experimental Botany*, **51**, 319–328.

Poolman, M.G., Kundu, S., Shaw, R. & Fell, D.A. (2013) Responses to light intensity in a genome-scale model of rice metabolism. *Plant Physiology*, **162**, 1060–1072.

Poolman, M.G., Miguet, L., Sweetlove, L.J. & Fell, D.A. (2009) A genome-scale metabolic model of Arabidopsis and some of its properties. *Plant Physiology*, **151**, 1570–1581.

Pozo, C., Miró, A., Guillén-Gosálbez, G., Sorribas, A., Alves, R. & Jiménez, L. (2015) Gobal optimization of hybrid kinetic/FBA models via outer-approximation. *Computers & Chemical Engineering*, **72**, 325–333.

Pries, C., Razaghi-Moghadam, Z., Kopka, J. & Nikoloski, Z. (2021) Integration of relative metabolomics and transcriptomics time-course data in a metabolic model pinpoints effects of ribosome biogenesis defects on *Arabidopsis thaliana* metabolism. *Scientific Reports*, **11**, 4787.

Rahimzadeh-Bajgiran, P., Tubuxin, B. & Omasa, K. (2017) Estimating chlorophyll fluorescence parameters using the joint Fraunhofer line depth and laser-induced saturation pulse (FLD-LISP) method in different plant species. *Remote Sensing*, **9**, 599.

Recht, L., Töpfer, N., Batushansky, A., Sikron, N., Gibon, Y., Fait, A. *et al.* (2014) Metabolite profiling and integrative modeling reveal metabolic constraints for carbon partitioning under nitrogen starvation in the green algae *Haematococcus pluvialis*. *Journal of Biological Chemistry*, **289**, 30387–30403.

Rogers, A., Allen, D.J., Davey, P.A., Morgan, P.B., Ainsworth, E.A., Bernacchi, C.J. *et al.* (2004) Leaf photosynthesis and carbohydrate dynamics of soybeans grown throughout their life-cycle under free-air carbon dioxide enrichment. *Plant, Cell & Environment*, **27**, 449–458.

Rohwer, J.M. & Botha, F.C. (2001) Analysis of sucrose accumulation in the sugar cane culm on the basis of in vitro kinetic data. *Biochemical Journal*, **358**, 437–445.

Sajitz-Hermstein, M., Töpfer, N., Kleessen, S., Fernie, A.R. & Nikoloski, Z. (2016) iReMet-flux: constraint-based approach for integrating relative metabolite levels into a stoichiometric metabolic models. *Bioinformatics*, **32**, i755–i762.

Scheible, W.-R., Gonzalez-Fontes, A., Lauerer, M., Muller-Rober, B., Caboche, M. & Stitt, M. (1997) Nitrate acts as a signal to induce organic acid metabolism and repress starch metabolism in tobacco. *The Plant Cell*, **9**, 783–798.

Scheunemann, M., Brady, S.M. & Nikoloski, Z. (2018) Integration of large-scale data for extraction of integrated Arabidopsis root cell-type specific models. *Scientific Reports*, **8**, 7919.

Schroeder, W.L. & Saha, R. (2020) Introducing an optimization- and explicit Runge-Kutta-based approach to perform dynamic flux balance analysis. *Scientific Reports*, **10**, 9241.

Sellers, P.J., Tucker, C.J., Collatz, G.J., Los, S.O., Justice, C.O., Dazlich, D.A. *et al.* (1996) A revised land surface parameterization (SiB2) for atmospheric GCMs. Part II: The generation of global fields of terrestrial biophysical parameters from satellite data. *Journal of Climate*, **9**, 706–737.

Shameer, S., Baghalian, K., Cheung, C.M., Ratcliffe, R.G. & Sweetlove, L.J. (2018) Computational analysis of the productivity potential of CAM. *Nature Plants*, **4**, 165–171.

Shameer, S., Ratcliffe, R.G. & Sweetlove, L.J. (2019) Leaf energy balance requires mitochondrial respiration and export of chloroplast NADPH in the light. *Plant Physiology*, **180**, 1947–1961.

Shameer, S., Vallarino, J.G., Fernie, A.R., Ratcliffe, R.G. & Sweetlove, L.J. (2020) Flux balance analysis of metabolism during growth by osmotic cell expansion and its application to tomato fruits. *The Plant Journal*, **103**, 68–82.

Shaw, R. & Cheung, C. (2018) A dynamic multi-tissue flux balance model captures carbon and nitrogen metabolism and optimal resource partitioning during Arabidopsis growth. *Frontiers in Plant Science*, **9**, 884.

Simons, M., Saha, R., Amiour, N., Kumar, A., Guillard, L., Clément, G. *et al.* (2014) Assessing the metabolic impact of nitrogen availability using a compartmentalized maize leaf genome-scale model. *Plant Physiology*, **166**, 1659–1674.

Siriwach, R., Matsuda, F., Yano, K. & Hirai, M.Y. (2020) Drought stress responses in context-specific genome-scale metabolic models of *Arabidopsis thaliana*. *Metabolites*, **10**, 159.

Smith, A.M. & Zeeman, S.C. (2006) Quantification of starch in plant tissues. *Nature Protocols*, **1**, 1342–1345.

South, P.F., Cavanagh, A.P., Liu, H.W. & Ort, D.R. (2019) Synthetic glycolate metabolism pathways stimulate crop growth and productivity in the field. *Science*, **363**, eaat9077.

Sun, J., Feng, Z., Leakey, A.D., Zhu, X., Bernacchi, C.J. & Ort, D.R. (2014) Inconsistency of mesophyll conductance estimate causes the inconsistency for the estimates of maximum rate of Rubisco carboxylation among the linear, rectangular and non-rectangular hyperbola biochemical models of leaf photosynthesis—A case study of CO_2 enrichment and leaf aging effects in soybean. *Plant Science*, **226**, 49–60.

Takagi, H., Watanabe, S., Tanaka, S., Matsuura, T., Mori, I.C., Hirayama, T. *et al.* (2018) Disruption of ureide degradation affects plant growth and development during and after transition from vegetative to reproductive stages. *BMC Plant Biology*, **18**, 287.

Tcherkez, G., Gauthier, P., Buckley, T.N., Busch, F.A., Barbour, M.M., Bruhn, D. *et al.* (2017) Leaf day respiration: low CO_2 flux but high significance for metabolism and carbon balance. *New Phytologist*, **216**, 986–1001.

Tcherkez, G. & Hodges, M. (2008) How stable isotopes may help to elucidate primary nitrogen metabolism and its interaction with (photo)respiration in C_3 leaves. *Journal of Experimental Botany*, **59**, 1685–1693.

Tcherkez, G., Mahé, A., Gauthier, P., Mauve, C., Gout, E., Bligny, R. *et al.* (2009) In folio respiratory fluxomics revealed by ^{13}C isotopic labeling and H/D isotope effects highlight the noncyclic nature of the tricarboxylic acid "cycle" in illuminated leaves. *Plant Physiology*, **151**, 620–630.

Töpfer, N., Braam, T., Shameer, S., Ratcliffe, R.G. & Sweetlove, L.J. (2020) Alternative CAM modes provide environment-specific water-saving benefits in a leaf metabolic model. *The Plant Cell*, **32**, 3689–3705.

Traub, M., Flörchinger, M., Piecuch, J., Kunz, H.H., Weise-Steinmetz, A., Deitmer, J.W. *et al.* (2007) The fluorouridine insensitive 1 (*fur1*) mutant is defective in equilibrative nucleoside transporter 3 (ENT3), and thus represents an important pyrimidine nucleoside uptake system in *Arabidopsis thaliana*. *The Plant Journal*, **49**, 855–864.

Uys, L., Botha, F.C., Hofmeyr, J.S. & Rohwer, J.M. (2007) Kinetic model of sucrose accumulation in maturing sugarcane culm tissue. *Phytochemistry*, **68**(16–18), 2375–2392.

Valle, E.M., Boggio, S.B. & Heldt, H.W. (1998) Free amino acid composition of phloem sap and growing fruit of *Lycopersicon esculentum*. *Plant and Cell Physiology*, **39**, 458–461.

von Caemmerer, S. (2000) *Biochemical models of leaf photosynthesis*. Collingwood, Vic: CSIRO Publishing.

Vos, J., Evers, J.B., Buck-Sorlin, G.H., Andrieu, B., Chelle, M. & De Visser, P.H. (2010) Functional–structural plant modelling: a new versatile tool in crop science. *Journal of Experimental Botany*, **61**, 2101–2115.

Walker, A. & Ho, L. (1977) Carbon translocation in the tomato: carbon import and fruit growth. *Annals of Botany*, **41**, 813–823.

Wang, Y., Long, S.P. & Zhu, X.-G. (2014) Elements required for an efficient NADP-malic enzyme type C_4 photosynthesis. *Plant Physiology*, **164**, 2231–2246.

Woodrow, I.E. & Mott, K.A. (1993) Modelling C_3 photosynthesis: A sensitivity analysis of the photosynthetic carbon-reduction cycle. *Planta*, **191**, 421–432.

Xu, Y., Fu, X., Sharkey, T.D., Shachar-Hill, Y. & Walker, B.J. (2021) The metabolic origins of non-photorespiratory CO_2 release during photosynthesis: A metabolic flux analysis. *Plant Physiology*, **58**, 7250–7257.

Yao, X., Zhou, H., Zhu, Q., Li, C., Zhang, H., Wu, J.-J. *et al.* (2017) Photosynthetic response of soybean leaf to wide light-fluctuation in maize-soybean intercropping system. *Frontiers in Plant Science*, **8**, 1695.

Yin, X. & Struik, P. (2009) C_3 and C_4 photosynthesis models: An overview from the perspective of crop modelling. *NJAS-Wageningen Journal of Life Sciences*, **57**, 27–38.

Yoon, D.-K., Ishiyama, K., Suganami, M., Tazoe, Y., Watanabe, M., Imaruoka, S. *et al.* (2020) Transgenic rice overproducing Rubisco exhibits increased yields with improved nitrogen-use efficiency in an experimental paddy field. *Nature Food*, **1**, 134–139.

Yuan, H., Cheung, C.M., Poolman, M.G., Hilbers, P.A. & van Riel, N.A. (2016) A genome-scale metabolic network reconstruction of tomato (*Solanum lycopersicum* L.) and its application to photorespiratory metabolism. *The Plant Journal*, **85**, 289–304.

Zaks, J., Amarnath, K., Kramer, D.M., Niyogi, K.K. & Fleming, G.R. (2012) A kinetic model of rapidly reversible nonphotochemical quenching. *Proceedings of the National Academy of Sciences*, **109**, 15757–15762.

Zhang, Y.-L., Hu, Y.-Y., Luo, H.-H., Chow, W.S. & Zhang, W.-F. (2011) Two distinct strategies of cotton and soybean differing in leaf movement to perform photosynthesis under drought in the field. *Functional Plant Biology*, **38**, 567–575.

Zhao, H.-L., Chang, T.-G., Xiao, Y. & Zhu, X.-G. (2021) Potential metabolic mechanisms for inhibited chloroplast nitrogen assimilation under high CO2. *Plant Physiology*, **187**(3), 1812–1833.

Zhu, X.-G., De Sturler, E. & Long, S.P. (2007) Optimizing the distribution of resources between enzymes of carbon metabolism can dramatically increase photosynthetic rate: a numerical simulation using an evolutionary algorithm. *Plant Physiology*, **145**, 513–526.

Zhu, X.-G., Long, S.P. & Ort, D.R. (2008) What is the maximum efficiency with which photosynthesis can convert solar energy into biomass? *Current Opinion in Biotechnology*, **19**, 153–159.

Zhu, X.-G., Long, S.P. & Ort, D.R. (2010) Improving photosynthetic efficiency for greater yield. *Annual Review of Plant Biology*, **61**, 235–261.

Zhu, X.G., Wang, Y., Ort, D.R. & Long, S.P. (2013) e-photosynthesis: a comprehensive dynamic mechanistic model of C_3 photosynthesis: from light capture to sucrose synthesis. *Plant, Cell & Environment*, **36**, 1711–1727.